MOLECULAR AND CELLULAR BIOLOGY, Jan. 2006, p. 140–154 Vol. 26, No. 1
0270-7306/06/$08.00+0 doi:10.1128/MCB.26.1.140–154.2006

Nox2 and Rac1 Regulate H_2O_2-Dependent Recruitment of TRAF6 to Endosomal Interleukin-1 Receptor Complexes†

Qiang Li,[1] Maged M. Harraz,[1] Weihong Zhou,[1] Liang N. Zhang,[1] Wei Ding,[1] Yulong Zhang,[1] Tim Eggleston,[1] Charles Yeaman,[1] Botond Banfi,[1] and John F. Engelhardt[1,2,3]*

Department of Anatomy and Cell Biology,[1] Department of Internal Medicine,[2] and Center for Gene Therapy of Cystic Fibrosis and Other Genetic Diseases,[3] College of Medicine, University of Iowa, Iowa City, Iowa 52242

Received 24 May 2005/Returned for modification 25 July 2005/Accepted 11 October 2005

Reactive oxygen species (ROS) generated by NADPH oxidases (Nox) have been implicated in the regulation of signal transduction. However, the cellular mechanisms that link Nox activation with plasma membrane receptor signaling remain poorly defined. We have found that Nox2-derived ROS influence the formation of an active interleukin-1 (IL-1) receptor complex in the endosomal compartment by directing the H_2O_2-dependent binding of TRAF6 to the IL-1R1/MyD88 complex. Clearance of both superoxide and H_2O_2 from within the endosomal compartment significantly abrogated IL-1β-dependent IKK and NF-κB activation. MyD88-dependent endocytosis of IL-1R1 following IL-1β binding was required for the redox-dependent formation of an active endosomal receptor complex competent for IKK and NF-κB activation. Small interfering RNAs to either MyD88 or Rac1 inhibited IL-1β induction of endosomal superoxide and NF-κB activation. However, MyD88 and Rac1 appear to be recruited independently to IL-1R1 following ligand stimulation. In this context, MyD88 binding was required for inducing endocytosis of IL-1R1 following ligand binding, while Rac1 facilitated the recruitment of Nox2 into the endosomal compartment and subsequent redox-dependent recruitment of TRAF6 to the MyD88/IL-1R1 complex. The identification of Nox-active endosomes helps explain how subcellular compartmentalization of redox signals can be used to direct receptor activation from the plasma membrane.

Receptor stimulation at the plasma membrane has been implicated in the production of cellular reactive oxygen species (ROS) by a significant number of ligands, including tumor necrosis factor alpha (TNF-α), lipopolysaccharide, angiotensin II, platelet-derived growth factor (PDGF), insulin, epidermal growth factor, transforming growth factor β1, and interleukin-1β (IL-1β) (40). Early studies demonstrated that enhanced cellular clearance of H_2O_2 by catalase abrogated PDGF and epidermal growth factor receptor signals, implicating H_2O_2 as a critical redox-signaling intermediate (3, 45). It is currently believed that H_2O_2 functions as a signaling intermediate by inhibiting cellular phosphatases at cysteines in the catalytic site (40) and by altering protein structure by oxidation of reactive thiols (15). For example, a recent study has implicated mitochondrial superoxide as a source of H_2O_2 responsible for the oxidative inactivation of JNK phosphatases important in TNF-mediated apoptosis (22). Similarly, peroxiredoxin II has been shown to act as a negative regulator of PDGF signaling by controlling the activity of protein tyrosine phosphatases important in PDGF receptor inactivation (7). In addition, cytosolic peroxiredoxin II attenuates the activation of JNK and p38 but potentiates ERK activation following TNF-α treatment (24).

The major ROS-generating systems in cells include the mitochondria and seven known NADPH oxidase catalytic subunits (Nox1, $Nox2^{gp91phox}$, Nox3, Nox4, Nox5, Duox1, and Duox2) (26). NADPH oxidases generate superoxide ($\cdot O_2^-$) by transferring an electron from NADPH to molecular oxygen. The most widely characterized NADPH oxidases include the phagocytic gp91phox (Nox2), which has also been found to be expressed in a variety of other nonphagocytic cell types (36, 47, 50). The active form of the phagocytic NADPH oxidase is composed of a multisubunit membrane complex. Subunit recruitment of p67phox, p47phox, p40phox, p22phox, and Rac1/2, a small GTPase, plays an important role in activating $\cdot O_2^-$ production for this complex (23, 26). Given the obvious potential toxicity of ROS, cells have also developed mechanisms to control both the production and clearance of ROS. Clearance of ROS is carefully regulated by a number of enzymes that dismutate $\cdot O_2^-$ to H_2O_2 (SOD-1, -2, and -3) or degrade H_2O_2 (glutathione peroxidases, catalase, and peroxiredoxins) (13, 41). As mentioned above, peroxiredoxin II is recruited to the PDGF receptor and regulates its phosphorylation status. In this context, peroxiredoxin II controls the availability of H_2O_2 which, in turn, regulates the activity of protein tyrosine phosphatases (7). This mechanism is an example of ROS-mediated regulation of signal transduction by the clearance of H_2O_2. On the contrary, cellular mechanisms that direct the production of Nox-derived superoxide to selectively influence certain receptor signaling pathways remain poorly understood.

A link between Nox protein activation and cellular signaling is only recently becoming recognized. For example, expression of a dominant negative Nox4 attenuates insulin-stimulated H_2O_2 production and downstream phosphatase signaling involved in adipocyte insulin receptor activation (32). TNF-α and IL-1β, two major proinflammatory cytokines well recognized for their abilities to activate NF-κB (16, 42), have also been hypothesized to utilize Nox-dependent H_2O_2 production in

* Corresponding author. Mailing address: Room 1-111 BSB, Department of Anatomy and Cell Biology, College of Medicine, University of Iowa, 51 Newton Road, Iowa City, IA 52242. Phone: (319) 335-7744. Fax: (319) 335-6581. E-mail: john-engelhardt@uiowa.edu.

† Supplemental material for this article may be found at http://mcb.asm.org/.

their activation cascades. Supportive evidence includes the demonstration that inhibition of Rac1 or p47phox abrogates TNF-α- and IL-1-stimulated H_2O_2 production and NF-κB activation (10, 14, 17, 21, 28). Similarly, enhanced clearance of H_2O_2 by GPx1 expression abrogates NF-κB activation (25, 29). However, the dependence of NF-κB activation on ROS still remains highly controversial (19). To this end, it is presently unclear how ligand binding to membrane receptors coordinates the production of ROS through NADPH oxidase(s) and downstream receptor signals that influence NF-κB activation.

IL-1β is a potent proinflammatory cytokine that plays an important role in many disease processes. IL-1β exerts its pleiotropic effects by binding to the IL-1 receptor (IL-1R1) on the plasma membrane and initiating the formation of an intracellular receptor-associated protein complex responsible for transducing receptor signals (35). Formation of an active IL-1R1 signaling complex involves the early binding of several accessory factors to the receptor, including IL-1RacP (20), MyD88 (34, 49), and Tollip (5). These factors then act in a context-dependent fashion to mediate the recruitment of IL-1 receptor-associated kinases (IRAK) (30, 34). Once associated with the receptor complex, IRAK subsequently leads to the recruitment of TRAF6, a member of the TNF receptor-associated factor (TRAF) family of adaptor proteins (38). TRAF6 is required for the activation and the recruitment of kinases such as TAK1 and NIK to the IL-1R1 complex (35, 38, 48). In the context of NF-κB activation, the IL-1R1 complex transmits signals through TAK1- and/or NIK-mediated phosphorylation of the IκB kinase (IKK) complex (16). Once the IKK complex is phosphorylated, it in turn phosphorylates IκBα/β, and NF-κB is mobilized to the nucleus.

In the present study, we have used the redox dependence of IL-1β-mediated NF-κB activation to study how Nox-derived ROS coordinate receptor signals required for efficient NF-κB activation. To this end, we have demonstrated that following IL-1β stimulation, MyD88-dependent endocytosis of IL-1R1 was required for the redox-dependent activation of NF-κB by the endosomal compartment. In the absence of endocytosis, the IL-1 receptor complex formation failed to incorporate TRAF6, and NF-κB activation was significantly abrogated. Similarly, clearance of ROS from within the endosomal compartment significantly retarded both IKK and NF-κB activation following IL-1β stimulation. ROS production by the endosomal compartment was facilitated by Rac1-dependent internalization of Nox2 with IL-1R1 and directed the H_2O_2-dependent recruitment of TRAF6 to ligand-activated IL-1R1/MyD88 complexes in endomembranes. Through this process, the generation of $\cdot O_2^-$ by endosomal Nox2, and its conversion to H_2O_2, facilitated the redox-dependent formation of an IL-1R1 complex capable of activating the IKK complex and NF-κB. This mechanism helps clarify how cells can partition Nox-derived ROS to selectively influence receptor activation from the plasma membrane.

MATERIALS AND METHODS

Recombinant expression vectors and small interfering RNA (siRNA). MCF-7 cells were infected with recombinant adenoviruses (500 particles/cell) as previously described, and cells were utilized for experiments at 48 h postinfection (29). Lipofectamine 2000 (Invitrogen) was used for all plasmid transfections, and cells were utilized for experiments at 48 h posttransfection. The following E1-deleted recombinant adenoviral vectors were used: (i) Ad.GPx-1, which encodes glutathione peroxidase 1 and degrades cytoplasmic H_2O_2 (29); (ii) Ad.Dyn(DN), which encodes a dominant-negative mutant (K44A) of dynamin and inhibits endocytosis (12); (iii) Ad.NFκBLuc, which encodes an NF-κB-responsive promoter driving luciferase expression and was used to assess NF-κB transcriptional activation in vivo (43); and (iv) Ad.BglII, an empty vector with no insert, as a control for viral infection (29). For NF-κB transcriptional assays utilizing infection with two recombinant adenoviruses, a slightly modified sequential infection method was used (43). In this case, cells were infected with experimental vectors [i.e., Ad.Dyn(DN) or Ad.GPx1] 24 h prior to infection with Ad.NFκBLuc, and cells were utilized for experiments at 48 h post-initial infection. Transduction efficiencies with recombinant adenoviruses were typically 80 to 90%, as assessed by Ad.CMV-GFP reporter gene expression.

The following plasmids were used for transient-transfection experiments: (i) a recombinant plasmid encoding an N-terminal hemagglutinin (HA) fusion of Rab5, generated by PCR amplification for immuno-affinity isolation of early endosomes, and (ii) an expression plasmid encoding the Nox2 cDNA, a kind gift from J. D. Lambeth (Emory University).

siRNAs against MyD88, Rac1, and Nox2 were obtained from Santa Cruz Biotechnology, and the transfections were performed using methods and reagents described by the manufacturer. The sequences used for the siRNAs were proprietary and were not provided by the company.

Cytokine treatments and vesicular isolation. MCF-7 cells were treated with recombinant IL-1β at the indicated concentrations for 20 min prior to all vesicular isolations. For endosomal loading experiments, purified bovine Cu/Zn superoxide dismutase (Cu/ZnSOD; Oxis Research) and/or catalase (Sigma-Aldrich) proteins were added to fresh medium (0.1 to 1 mg protein/ml) and applied to cells 10 min prior to cytokine treatment in the continued presence of SOD and/or catalase. Cells were washed and scraped into ice-cold phosphate-buffered saline (PBS). Cell pellets were then resuspended in 0.5 ml of homogenization buffer (0.25 M sucrose, 10 mM triethanolamine, 1 mM EDTA, 1 mM phenylmethylsulfonyl fluoride, and 100 μg/ml aprotinin), homogenized in a Duall tissue grinder (Duall), and centrifuged at 2,000 × *g* at 4°C for 10 min. The supernatant was designated the postnuclear supernatant (PNS). The PNS was subsequently combined with 60% Iodixanol (OptiPrep Axis-Shield) solution to obtain a final concentration of 32% and loaded into an sw55Ti centrifuge tube. The PNS was then bottom loaded under two-step gradients of 24% and 20% Iodixanol in homogenization buffer. Samples were centrifuged at 30,500 rpm for 2 h at 4°C. Fractions were collected from the top to the bottom of the centrifuge tube at 4°C (~300 μl per fraction) and utilized immediately for NADPH oxidase activity and immuno-isolation or were frozen for Western blot analysis.

NF-κB and NADPH oxidase activity assays. NF-κB transcriptional activity was assessed using the previously described NF-κB-inducible luciferase reporter vector (Ad.NFκBLuc) (43). Luciferase activity was assessed at 6 h post-cytokine treatment (unless otherwise specified) using 5 μg of cell lysate. NADPH oxidase activities were analyzed by measuring the rate of $\cdot O_2^-$ generation using a chemiluminescent, lucigenin-based system (31). Prior to the initiation of the assay, 5 μg of vesicular proteins was combined with 5 μM lucigenin (Sigma-Aldrich) in PBS and incubated in darkness at room temperature for 10 min. The reaction was initiated by the addition of 100 μM of NADPH (Sigma-Aldrich), and changes in luminescence were measured over the course of 3 min (five readings/s). The slope of the luminescence curve (relative light units [RLU] per minute) ($r > 0.95$) was used to calculate the rate of $\cdot O_2^-$ formation as an index of NADPH oxidase activity (RLU/min μg protein). In the absence of NADPH, background levels of lucigenin-dependent luminescence were always >1,000-fold less than maximally induced values in the presence of NADPH. Additionally, background levels of luminescence in the absence of NADPH did not significantly vary between samples and had no rate of change.

Electron spin resonance spectroscopy (ESR) was used to confirm the production of NADPH-dependent $\cdot O_2^-$ by isolated endosomes. ESR assays were conducted at room temperature using a Bruker model EMX ESR spectrometer (Bruker). Vesicular fractions from each sample were mixed with the spin trap, 50 mM 5,5-dimethyl-1-pyrroline *N*-oxide (DMPO), in a total volume of 500 μl of PBS, pH 7.4. This solution contained iminodiacetic acid-chelating resin (10 ml/liter; Sigma-Aldrich). The reaction was initiated by adding NADPH to 100 μM and was immediately placed into the ESR spectrometer. DMPO-hydroxyl radical adduct formation was assayed for 10 min. Instrument settings were as follows: receiver gain, 1×10^6; modulation frequency, 100 kHz; microwave power, 40.14 mW; modulation amplitude, 1.0 G; and sweep rate, 1 G/s.

Vesicular immuno-isolation. Rab5-containing endosomes were isolated based on a previous method (46). Cells were transfected with HA-Rab5a or green fluorescent protein (GFP) expression plasmid 48 h prior to IL-1β treatment. Following Iodixanol isolation of intracellular vesicles, one-half of the combined

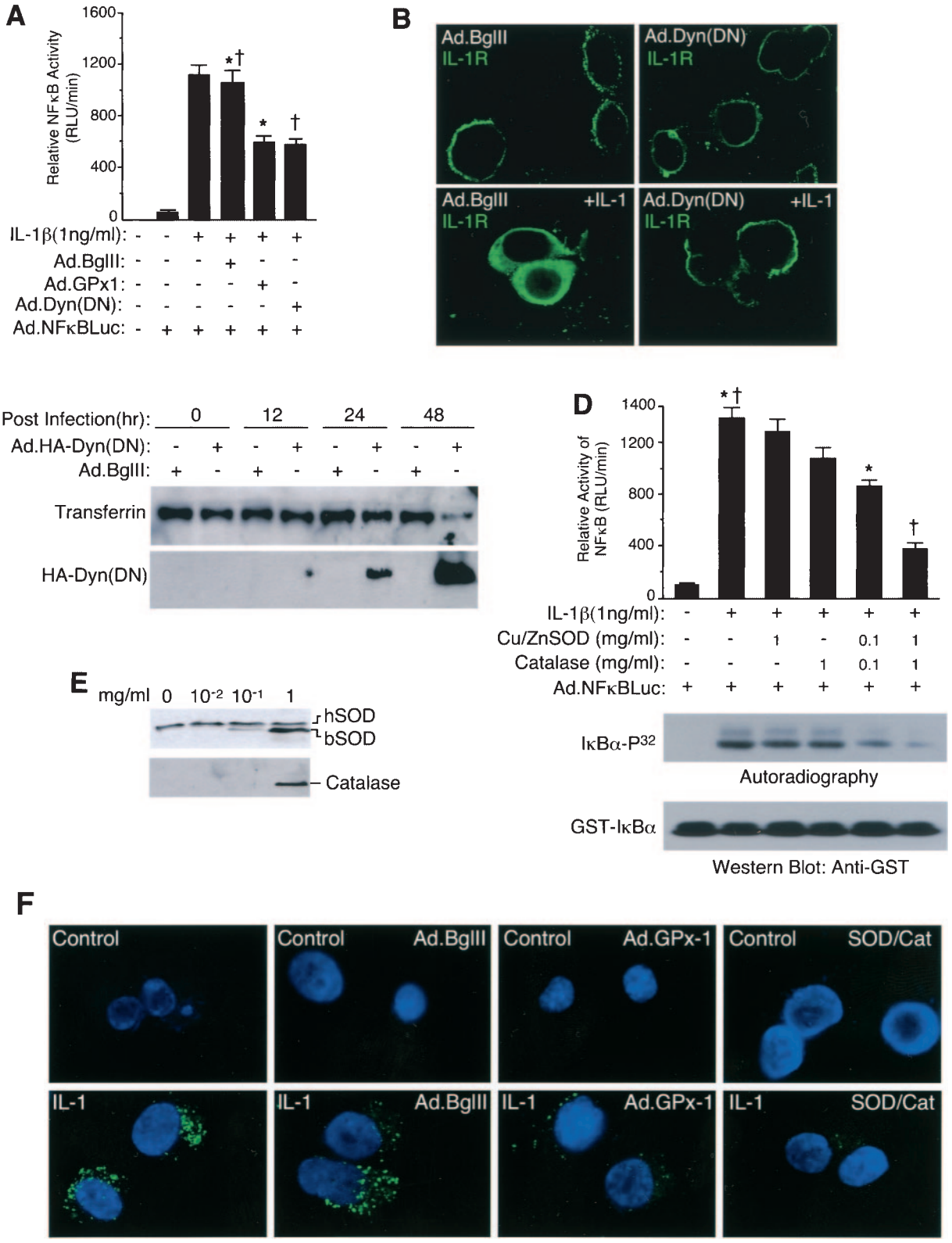

FIG. 1. Redox regulation of NF-κB activation is dependent on endocytosis. (A and D) MCF-7 cells were infected with the indicated adenoviral vectors and/or treated with the indicated concentrations of purified bovine Cu/ZnSOD and/or catalase proteins prior to cytokine treatment and assessment of NF-κB transcriptional activity at 6 h post-cytokine treatment (mean ± standard error [SE]; $n = 3$). Paired comparisons (*, †) demonstrate significant differences ($P < 0.05$). Bottom panel of D: IKKα activity was assessed using immunoprecipitated IKKα and in vitro kinase assays with [γ-^{32}P]ATP and GST-IκBα, followed by SDS-PAGE, transfer to nitrocellulose, autoradiography, and then Western blotting with anti-GST antibody. (B) Immunofluorescent localization of IL-1R1 in MCF-7 cells infected with Ad.Dyn(DN) (dominant-negative dynamin) or

peak vesicular fraction was used directly for biochemical analyses, and the other half was used for immuno-affinity isolation using Dynabeads M-500 (Dynal Bioscience) coated with the anti-HA antibody. Prior to use, beads were coated with antibodies as follows: the secondary antibody (anti-rat antibody) was conjugated to Dynabeads (4×10^8 beads/ml) in 0.1 M borate buffer (pH 9.5) for 24 h at 25°C with slow rocking. The beads were then placed into the magnet for 3 min and washed in 0.1% (wt/vol) bovine serum albumin (BSA)–PBS for 5 min at 4°C. A final wash in 0.2 M Tris (pH 8.5)–BSA was performed for 24 h. Finally, the beads were resuspended in BSA-PBS and conjugated to 4 μg of primary anti-HA antibody per 10^7 beads overnight at 4°C and then washed in BSA-PBS. Vesicular fractions were mixed with 700 μl of coated beads in PBS containing 2 mM EDTA, 5% BSA, and protease inhibitors. The mixture was incubated for 6 h at 4°C with slow rocking, followed by magnetic capture and washing in the same tube three times (15 min each). Beads with HA-enriched endosomes were then resuspended in PBS, and wash supernatants were saved for analysis.

Western blotting, immunoprecipitations, and in vitro kinase assays. Western blotting was performed using standard protocols (8), and protein concentrations were determined using the Bio-Rad protein quantification kit. Immunoreactive proteins were detected using enhanced chemiluminescence (ECL; Amersham) and were exposed to X-ray film. Antibodies used for Western blotting were as follows: anti-early endosomal antigen 1 (anti-EEA1), anti-HA, anit-Rab5, and anti-Rab11 antibodies (Transduction Laboratories); anti-p47phox, anti-TRAF6, anti-IKKα, anti-Na^+/K^+ ATPase(α3), anti-MyD88, and anti-glutathione *S*-transferase (anti-GST) antibodies (Santa Cruz Biotech); anti-IL-1R1 antibody (QED Bioscience, Inc.); anti-Cu/ZnSOD and anticatalase antibodies (Binding Site, Inc.); and anti-mtHSP70 antibody (Affinity Bioreagents). The Nox2 antibody was a kind gift from A. Jesaitis (Montana State University) (6).

For immunoprecipitations, cells were washed with ice-cold PBS and lysed in radioimmunoprecipitation assay (RIPA) buffer at 4°C for 30 min. A 500-μg aliquot of cellular protein and 5 μl of primary antibody were mixed with 1 ml of RIPA buffer at 4°C for 1 h. A 50-μl volume of protein A-agarose beads (Santa Cruz Biotech) was then added to the mixture and rotated for 4 h. The beads were washed with ice-cold PBS prior to experimental analyses. In vitro kinase assays were performed with immunoprecipitated IKKα and/or isolated vesicles using GST-IκBα as a substrate. Kinase reactions were performed with 1 μg GST-IκBα, 0.3 mM cold ATP, and 10 μCi [γ-^{32}P]ATP in 10 μl kinase buffer (40 mM HEPES, 1 mM β-glycerophosphate, 1 mM nitrophenolphosphate, 1 mM Na_3VO_4, 10 mM $MgCl_2$, and 2 mM dithiothreitol). The reaction mixtures were then incubated at 30°C for 30 min. Reactions were terminated by the addition of sodium dodecyl sulfate-polyacrylamide gel electrophoresis (SDS-PAGE) protein-loading buffer and boiled at 98°C for 5 min. Following SDS-PAGE, gels were transferred to nitrocellulose membranes and exposed to X-ray film prior to probing with an anti-GST antibody.

In vivo localization of redox-active endosomes and ROS production. In vivo localization of $\cdot O_2^-$ within endosomes was performed using OxyBURST Green dihydro-2′,4,5,6,7,7′-hexafluorofluorescein (H_2HFF)–BSA (Molecular Probes). Stock solutions (1 mg/ml) were generated immediately prior to use by dissolving H_2HFF-BSA in PBS under nitrogen and protected from light. Cells were incubated in the presence of 50 μg/ml OxyBurst Green H_2HFF-BSA for 2 min at 37°C and then stimulated by the addition of IL-1β (1 ng/ml). Cells were fixed in 4% paraformaldehyde at various times (1 to 10 min) poststimulation and evaluated by fluorescent microscopy. Various compounds (1 mg/ml SOD or 10 μM diphenylene iodonium [DPI]) were added at the time of IL-1β stimulation. Colocalization of H_2HFF-BSA and EEA1 was performed by immunofluorescent localization in postfixed samples using an anti-EEA1 monoclonal antibody (Transduction Laboratories) and a Texas Red-conjugated goat anti-mouse antibody (Jackson ImmunoResearch Laboratories). In vivo localization of total cellular ROS (predominantly H_2O_2) was performed using H_2DCFDA (Molecular Probes). Stock solutions of H_2DCFDA were generated in dimethyl sulfoxide at a concentration of 50 μg/ml immediately prior to use. Cells were washed three times with PBS prior to the simultaneous treatment with H_2DCFDA (10 μM) and IL-1β (1 ng/ml) for 20 min in PBS at 37°C in the dark. For samples infected with adenoviral vectors, this was done 48 h prior to stimulating with IL-1β. When SOD/catalase proteins were added to the medium, this was done at a concentration of 1 mg/ml at the time of IL-1β stimulation. Following washing and fixation for 10 min in 4% paraformaldehyde, cells were mounted in 4′,6′-diamidino-2-phenylindole (DAPI) containing antifadent and examined by fluorescence microscopy for DCF signal.

RESULTS

Endocytosis and endosomal ROS play key roles in IL-1β-mediated NF-κB activation. We evaluated IL-1β induction of NF-κB in an epithelial cell line (MCF-7) as a model for studying redox-sensitive signal transduction. This model demonstrated that IL-1β induction of a transcriptional NF-κB luciferase reporter was significantly inhibited (~50%) by recombinant adenovirus-mediated overexpression of GPx-1 (which degrades H_2O_2 to H_2O in the cytoplasm) (Fig. 1A). In these studies, approximately 85% of cells were transduced with recombinant adenovirus as determined using a GFP reporter (data not shown). Similarly, partial inhibition of endocytosis by overexpression of Ad.Dyn(DN) (9) (Fig. 1B and C) also inhibited NF-κB to a similar extent (Fig. 1A). These findings suggested that ROS production and endocytosis were equally required for a significant fraction of NF-κB activation by IL-1β.

Endocytosis of ligand-bound receptors is often intricately linked to the processing and propagation of intracellular signals (44). However, the potential links between receptor processing and redox-dependent activation in the endosome have not been previously investigated. Based on the results from Fig. 1A, we hypothesized that endosome-derived ROS production following IL-1β stimulation might be responsible for amplifying receptor/effector activation through a redox-dependent process. To this end, we investigated whether ROS clearance from the endosomal compartment might also influence NF-κB activation. Purified Cu/ZnSOD and catalase proteins were efficiently taken up by MCF-7 cells when added to the medium at a 1-mg/ml concentration (Fig. 1E). Indeed, cellular uptake of Cu/ZnSOD and catalase by MCF-7 cells significantly reduced both IKK and NF-κB activation by IL-1β in a dose-dependent fashion (Fig. 1D). The synergistic ability of Cu/ZnSOD and catalase to inhibit IKK and NF-κB activation together, more effectively than either alone, suggested that both endosomal $\cdot O_2^-$ and H_2O_2 were likely involved in IL-1R1 complex activation. Furthermore, overexpression of cytoplasmic GPx-1 also inhibited NF-κB activation and suggested that H_2O_2 was a likely redox second messenger of the NF-κB pathway. To confirm that GPx-1 expression and cellular loading with Cu/ZnSOD/catalase both reduced cellular ROS

Ad.BglII (empty control vector) 48 h prior to treatment with IL-1β. Note that fixation conditions necessary for IL-1R1 staining lead to vesicle membrane breakdown and intracellular dispersal of signal. (C) MCF-7 cells were infected with Ad.Dyn(DN) (HA tagged) or Ad.BglII at various times prior to biotin-transferrin being added to the medium for 30 min. Cells were trypsinized, and cell lysates were evaluated by Western blotting with anti-HA antibody or avidin-horseradish peroxidase. (E) Loading of MCF-7 cells with various concentrations of purified bovine Cu/ZnSOD or catalase added to the medium for 20 min. Cells were trypsinized following treatment, and cell lysates were evaluated by Western blotting for uptake of enzymes. hSOD, endogenous human Cu/ZnSOD; bSOD, bovine Cu/ZnSOD. (F) MCF-7 cells were infected with the indicated adenoviral vectors 48 h prior to IL-1β (1 ng/ml) treatment in the presence of H_2DCFDA (10 μM). Additionally, cells were simultaneously treated with 1 mg/ml bovine Cu/ZnSOD and catalase proteins at the time of H_2DCFDA and IL-1β treatment. Control cells were not treated with IL-1β. Cells were washed and fixed at 20 min poststimulation and mounted in DAPI containing antifadent prior to fluorescence microscopy. Green DCF fluorescence is an indicator of H_2O_2 levels, and DAPI blue fluorescence marks nuclei.

following IL-1β treatment, we used a ROS-sensitive dye (H_2DCFDA) to assess the level of cellular ROS under the various treatment conditions. As shown in Fig. 1F, IL-1β treatment stimulated cellular ROS, and expression of GPx-1 and cellular loading with Cu/ZnSOD/catalase both inhibited DCF fluorescence. These findings led us to investigate the mechanism of ROS generation within the endosomal compartment and how such ROS might influence the IL-1R1 complex to become competent for IKK complex activation.

IL-1β stimulates endosomal NADPH-dependent $\cdot O_2^-$ production required for TRAF6 recruitment. We hypothesized that Nox complexes within ligand-activated endosomes might serve as sources of the ROS required for IL-1β-mediated NF-κB activation. To this end, we investigated whether IL-1β could stimulate NADPH-dependent $\cdot O_2^-$ production in vesicular fractions of MCF-7 cells. Peak vesicular fractions isolated by Iodixanol density gradient centrifugation expressed Rab5 and Rab11, two vesicular markers of early and recycling endosomes, respectively (51) (Fig. 2A, fractions 3 and 4). They also contained internalized biotin-transferrin, as would be expected for this compartment. However, vesicular fractions were devoid of mitochondrial mtHSP70, plasma membrane Na^+/K^+-ATPase, or peroxisomal catalase, demonstrating little, if any, contamination from these compartments (Fig. 2A). In contrast, peak Rab5/11 vesicular fractions demonstrated significant overlap with endoplasmic reticulum, Golgi, and lysosomal enzymes, as would be expected from this isolation strategy (see Fig. S1 in the supplemental material).

Using a lucigenin-based chemiluminescence assay to detect $\cdot O_2^-$ production in the various Iodixanol fractions (31), we assessed the rate of NADPH-dependent $\cdot O_2^-$ production as an index of Nox activity. As hypothesized, IL-1β stimulation significantly increased NADPH-dependent $\cdot O_2^-$ production in peak vesicular fractions 3 and 4 (Fig. 2B). Having established that IL-1β induces the formation of NADPH oxidase-active endosomes, we next sought to establish that $\cdot O_2^-$ was generated in the lumen of isolated IL-1β-activated endosomes, as predicted by the ability of endocytosed ROS-scavenging enzymes to inhibit IKK/NF-κB activation (Fig. 1D). To address this question, we evaluated the ability of Cu/ZnSOD protein in the medium to be taken up into endosomes and degrade $\cdot O_2^-$ from the interior of isolated endosomes. Since lucigenin, but not Cu/ZnSOD protein, is membrane permeable, the extent to which $\cdot O_2^-$ was produced in the interior of endosomes could be determined using the lucigenin-based chemiluminescence assay. Biochemical studies confirmed that when the Cu/ZnSOD protein was added to the medium [SOD(m)], it was indeed internalized into isolated endosomes and remained resistant to pronase digestion (Fig. 2C). In contrast, Cu/ZnSOD added to the exterior of unloaded isolated endosomes [SOD(v)] was effectively degraded by pronase. As expected, disruption of endosomal membranes with Triton X-100 sensitized intralumenal Cu/ZnSOD [SOD(m)] to pronase degradation. Hence, Cu/ZnSOD protein in the medium is indeed taken up into the endosomal compartment. An unexpected finding from these bovine Cu/ZnSOD endosomal-loading experiments was the IL-1β-dependent recruitment of endogenous cellular human Cu/ZnSOD protein to vesicular membranes (Fig. 2C, lane 5 versus 6). This cellular human Cu/ZnSOD was sensitive to pronase digestion in the absence of Triton X-100, demonstrating that it resided on the endosomal surface. These findings suggest the intriguing possibility that Cu/ZnSOD may play an active role in ROS metabolism at the endosomal level following IL-1β stimulation.

The ability of intralumenal Cu/ZnSOD to inhibit IL-1β-induced $\cdot O_2^-$ production by isolated vesicles suggested that the majority of $\cdot O_2^-$ was generated from within the interior of isolated endosomes (Fig. 2D). The addition of KCN (Cu/ZnSOD inhibitor) to the lucigenin reaction completely reversed this inhibition (Fig. 2D) and demonstrated that the inhibitory effect was specifically due to enzymatic Cu/ZnSOD activity. Enhanced NADPH-dependent production of $\cdot O_2^-$ by IL-1β-activated endosomes was also confirmed using ESR (Fig. 2E). In this context, DMPO adduct formation was completely inhibited by endosomal loading with Cu/ZnSOD, but not catalase, prior to vesicular isolation and ESR analysis. This finding demonstrated that $\cdot O_2^-$, not H_2O_2, was the predominant ROS leading to ESR signal. NADPH-dependent $\cdot O_2^-$ production in peak vesicular fractions was also sensitive to DPI, (an NADPH oxidase inhibitor), but not to rotenone (Fig. 2F) or antimycin A (see Fig. S2 in the supplemental material) (specific inhibitors of mitochondrial electron transport chain complex I or III, respectively). These findings ruled out significant mitochondrial contamination as the source of ROS generation in the vesicular fractions. IL-1β stimulation of endosomal $\cdot O_2^-$ was also dependent on endocytosis, as demonstrated by a 75% reduction in the presence of Ad.Dyn(DN) infection but not following infection with an empty vector control adenovirus (Fig. 2G). Such a reduction closely mirrored the extent of inhibition of transferrin uptake following Ad.Dyn(DN) infection (Fig. 1C). Cumulatively, these studies and the fact that endosomal loading with Cu/ZnSOD/catalase significantly reduced IL-1β-stimulated DCF fluorescence (Fig. 1F) suggest that IL-1β induces $\cdot O_2^-$ and H_2O_2 production in MCF-7 cells predominantly within an endosomal compartment following receptor endocytosis.

Given the ability of ROS clearance from inside the endosomal compartment to inhibit IKK and NF-κB activation by IL-1β (Fig. 1D), we hypothesized that redox-active endosomes might provide the subcellular framework for spatially controlled redox-dependent activation of the IL-1R complex. MyD88 is well recognized as one of the first effectors recruited to IL-1R1 following ligand binding. This process stimulates an ordered recruitment of effectors and adaptors (IL-1R1 → MyD88 → IRAK → TRAF6), which ultimately leads to the formation of an active IKK kinase complex capable of activating NF-κB (16). Using endosomal loading with SOD and catalase, the redox dependence of MyD88 and TRAF6 recruitment to the endosomal compartment following IL-1β stimulation was evaluated in purified vesicular fractions. Results from these experiments demonstrated that TRAF6 recruitment to the endosomal compartment following IL-1β stimulation was reduced ~50% by endosomal loading of SOD/catalase (Fig. 2H), a finding which closely mirrored the reduction in total cellular IKK kinase activity under similar conditions (Fig. 1D). In contrast, endosomal loading of ROS clearance enzymes did not alter MyD88 recruitment to the endosomal fraction following IL-1β stimulation (Fig. 2H). These findings suggested the recruitment of TRAF6 to IL-1R1 might occur in a redox-dependent fashion at the level of the endosome.

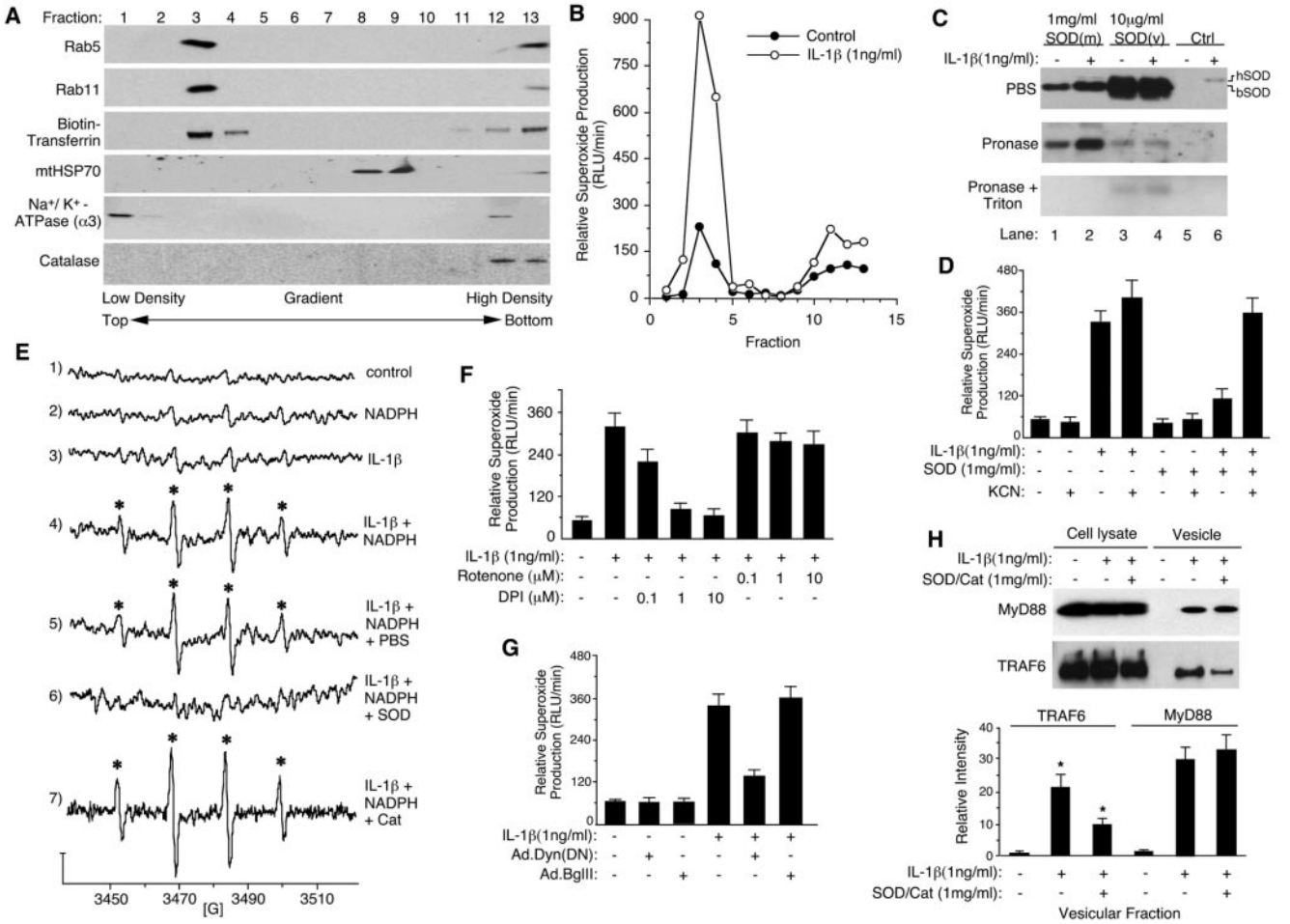

FIG. 2. IL-1β stimulates endosomal NADPH-dependent $\cdot O_2^-$ production required for TRAF6 recruitment. (A) MCF-7 cell vesicular fractionation on Iodixanol gradients was performed following treatment with IL-1β and biotin-transferrin for 20 min. Each fraction was evaluated by Western blotting for the various molecular markers as indicated. (B) NADPH-dependent $\cdot O_2^-$ production following IL-1β stimulation was assessed in each Iodixanol fraction in a lucigenin-based chemiluminescence assay. (C) MCF-7 cell vesicular fractions from SOD(m) (bovine Cu/ZnSOD protein was added to the cellular medium prior to vesicular isolation), SOD(v) (bovine Cu/ZnSOD was added to vesicular fractions following isolation), and control (Ctrl; no Cu/ZnSOD addition) treatment conditions were incubated with PBS, pronase, or pronase plus Triton X-100 (0.5%) at 37°C for 30 min. The samples were then separated by SDS-PAGE and analyzed by Western blotting using an anti-Cu/ZnSOD antibody. hSOD, human Cu/ZnSOD; bSOD, bovine Cu/ZnSOD. (D) MCF-7 cells were loaded with purified bovine Cu/ZnSOD at the time of cytokine treatment, and NADPH-dependent $\cdot O_2^-$ production in the peak vesicular fractions (no. 2 to 4) was evaluated using lucigenin in the presence or absence of 50 μM KCN (Cu/ZnSOD inhibitor) (mean ± SE; $n = 3$). (E) $\cdot O_2^-$ production in the peak vesicular fractions was evaluated by ESR using the spin-trap DMPO in the presence and absence of 100 μM of NADPH (conditions 1 to 4). Assays were also performed with isolated vesicular fractions loaded with Cu/ZnSOD or catalase proteins (conditions 5 to 7). Asterisks mark DMPO/˙OH adducts. The y axis represents 5×10^4 arbitrary units of intensity, and the x axis represents the magnetic field in Gauss. (F) Pooled vesicular fractions (2 to 4) were evaluated for NADPH-dependent $\cdot O_2^-$ production in the absence or presence of DPI (Nox inhibitor) or rotenone (mitochondrial respiratory chain complex I inhibitor). (G) The vesicular fractions (2 to 4) were evaluated for NADPH-dependent $\cdot O_2^-$ production from cells infected with dynamin(K44A)-expressing or empty vector (Ad.BglII) recombinant adenovirus prior to IL-1β stimulation. (H) MCF-7 cells were loaded with Cu/ZnSOD/catalase protein and treated with IL-1β for 20 min. Whole-cell lysates or purified vesicular fractions were evaluated by Western blotting for MyD88 and TRAF6 (upper panel). Infrared quantification of MyD88 and TRAF6 band intensities from the vesicular fractions are plotted in the lower panel (mean ± SE; $n = 3$). *, Student's t test demonstrated a significant reduction in endosomal TRAF6 in the presence of Cu/ZnSOD/catalase loading ($P < 0.05$).

IL-1β induces Nox2 complex activation in the endosomal compartment. Having established that IL-1β induces $\cdot O_2^-$ production by the endosomal compartment in an NADPH-dependent fashion, we next sought to identify a candidate Nox enzyme(s) that might be responsible for endosomal $\cdot O_2^-$ production. Since Nox activation in the endosomal compartment was largely dependent on endocytosis (Fig. 2G), we hypothesized that specific subunits of the NADPH-oxidase complex would likely be recruited into endosomes following ligand stimulation. Reverse transcription-PCR analysis for Nox1, -2, -3, -4, and -5 mRNA in MCF-7 cells demonstrated that only Nox2 and Nox5 mRNA expression could be detected in this cell line (see Fig. S3 in the supplemental material). Subsequent analysis of purified endosomes demonstrated that IL-1β stimulation promoted the recruitment of three known Nox2 activators (Rac1, p67phox, and p47phox) to endomembranes (Fig.

3A). Furthermore, inhibiting endocytosis through the expression of dynamin(K44A) [i.e., following Ad.Dyn(DN) infection], significantly attenuated IL-1β-mediated recruitment of Rac1, p67phox, and p47phox to the vesicular fraction (Fig. 3A). These findings suggested that membrane internalization following IL-1β stimulation was required for the formation of an active endosomal Nox complex. They also substantiated earlier findings that endocytosis was required for IL-1β induction of $\cdot O_2^-$ by the endosomal compartment (Fig. 2G).

We next evaluated how endosomal $\cdot O_2^-$ and/or H_2O_2 might influence the recruitment of various IL-1R1 (MyD88 and TRAF6) or Nox (Rac1, p67phox, and p47phox) effectors to the endosomal compartment following ligand stimulation. To this end, we loaded endosomes at the time of IL-1β stimulation by the addition of SOD or SOD/catalase to the medium and evaluated the recruitment of these various effectors to isolated endosomes. Results from these experiments (Fig. 3A) demonstrated that only the SOD/catalase combination inhibited recruitment of TRAF6 to endosomes following IL-1β stimulation. The lack of a functional effect with SOD loading alone suggested that H_2O_2 is the primary ROS effector required for the recruitment of TRAF6 to the endosome. In contrast, the recruitment of MyD88, Rac1, p67phox, or p47phox to IL-1β-activated endosomes remained unaffected by SOD or SOD/catalase loading. Kinetic analysis of IL-1R1, Nox2, MyD88, and TRAF6 recruitment into endosomes (Fig. 3B) demonstrated that maximal endocytosis of IL-1R1 occurred by 15 to 30 min following IL-1 treatment, concordant with MyD88 recruitment. TRAF6 recruitment to endosomes lagged maximal levels of Nox2 in the endosomal compartment, as expected if Nox2-derived ROS were required to facilitate TRAF6 binding to the IL-1R1 endosomal complex. Interestingly, Nox2 was cleared more rapidly from the endosomal compartment than IL-1R1, suggesting that endosomal processing removes Nox2 after maximal recruitment of TRAF6 has occurred. Loading of SOD/catalase reduced TRAF6 recruitment to endosomes at all time points but did not affect IL-1R1, Nox2, or MyD88 levels in the endosome. Cumulatively, these studies and those in Fig. 2G suggest that activation of endosomal Nox complexes following IL-1β stimulation is dependent on endocytosis from the plasma membrane and that this process influences the redox-dependent recruitment of TRAF6 to its endosomal ligand-activated receptor complex.

Rac1, p67phox, and p47phox have all been associated as coactivators of Nox1 and -2, but not Nox3, -4, or -5 (26, 37). Given the fact that only Nox5 and Nox2 mRNA expression was detected in MCF-7 cells (see Fig. S3 in the supplemental material), we hypothesized that Nox2 might be responsible for ROS production by the endosomal compartment following IL-1β stimulation. We attempted to address this hypothesis using two approaches. Our first approach involved attempting to modulate endosomal ROS production by ectopically overexpressing Nox2 using transient transfection. As shown in Fig. 3C, ectopic expression of Nox2 significantly enhanced NADPH-dependent $\cdot O_2^-$ production by isolated IL-1β-stimulated endosomes in comparison to transfection with an irrelevant pcDNA plasmid. Furthermore, overexpression of Nox2 significantly enhanced Nox2 incorporation into endosomes only following IL-1β-stimulation (Fig. 3D, lane 5 versus 8). Although the levels of endogenous Nox2 were extremely low in MCF-7 cells, these studies also demonstrated enhanced recruitment of endogenous Nox2 to endosomes only following IL-1β stimulation (Fig. 3D, lane 6 versus 9, longer exposure lanes). Using a second approach, we also demonstrated that Nox2 siRNA, but not an irrelevant scrambled siRNA, significantly inhibited Nox2 protein expression in MCF-7 cells and NADPH-dependent $\cdot O_2^-$ production by isolated IL-1β-stimulated endosomes (Fig. 3E). Furthermore, Nox2 siRNA significantly reduced recruitment of both ectopically expressed and endogenous Nox2 to the endosomal compartment following IL-1β stimulation (Fig. 3F). Nox2 siRNA, but not scrambled siRNA, also attenuated IL-1β-induced NF-κB transcriptional activation (Fig. 3G) and endosomal NADPH-dependent superoxide production (Fig. 3E) to similar extents. Cumulatively, these studies provide strong molecular and functional confirmation that Nox2 complexes are activated in IL-1β-stimulated endosomes.

IL-1β induces Nox2 complex activation in early endosomes. Based on the finding that ligand-stimulated endocytosis was required for Nox2 activation in the endosomal compartment, we next hypothesized that the formation of these redox-active endosomes likely initiated at the level of the early endosome. To investigate this hypothesis, we probed for ROS production in the early endosomal compartment using a membrane-impermeable BSA-conjugated fluorescent dye H_2HFF-BSA. By incubating cells in the presence of H_2HFF-BSA, we were able to load the endosomal compartment with this dye and detect $\cdot O_2^-$ by a green fluorescence signal. These studies demonstrated a dramatic increase in the H_2HFF-BSA endosomal fluorescence following IL-1β treatment for 10 min (Fig. 4A and B). IL-1β-induced H_2HFF-BSA fluorescence was significantly inhibited by treating cells with DPI or loading purified Cu/ZnSOD protein into the endosomal compartment (Fig. 4C and D). These findings confirmed that Nox-derived $\cdot O_2^-$ was the major ROS detected by H_2HFF-BSA in the endosomal compartment. Colocalization studies with H_2HFF-BSA and EEA1 demonstrated that IL-1β significantly increased the abundance of EEA1- and H_2HFF-BSA-copositive endosomes (Fig. 4F) compared to unstimulated cells (Fig. 4E). Additionally, IL-1β stimulation led to an increase in H_2HFF-BSA-positive endosomes that did not contain EEA1; however, this population was less abundant at early time points poststimulation and increased with time. These findings are consistent with the notion that the ligand-stimulated $\cdot O_2^-$-producing redox-active endosomes are originated in the EEA1 compartment, while retaining some ability to produce $\cdot O_2^-$ after being processed into downstream endosomal compartments.

To provide additional biochemical confirmation for redox-active endosome formation in the early endosomal compartment following IL-1β stimulation, we purified early Rab5-positive endosomes using an immuno-affinity isolation procedure. Rab5, an early endosome-specific GTPase, plays a critical role in trafficking and membrane fusion of the early endosome. Purification of this compartment was facilitated by the overexpression of a recombinant HA-tagged Rab5 and immuno-affinity isolation from Iodixanol-isolated endosomes using anti-HA antibodies linked to Dynabeads. Results from these immuno-affinity isolation experiments (Fig. 4G and H) demonstrated that a significant portion of Nox activity (i.e., NADPH-dependent $\cdot O_2^-$ production) was associated with the

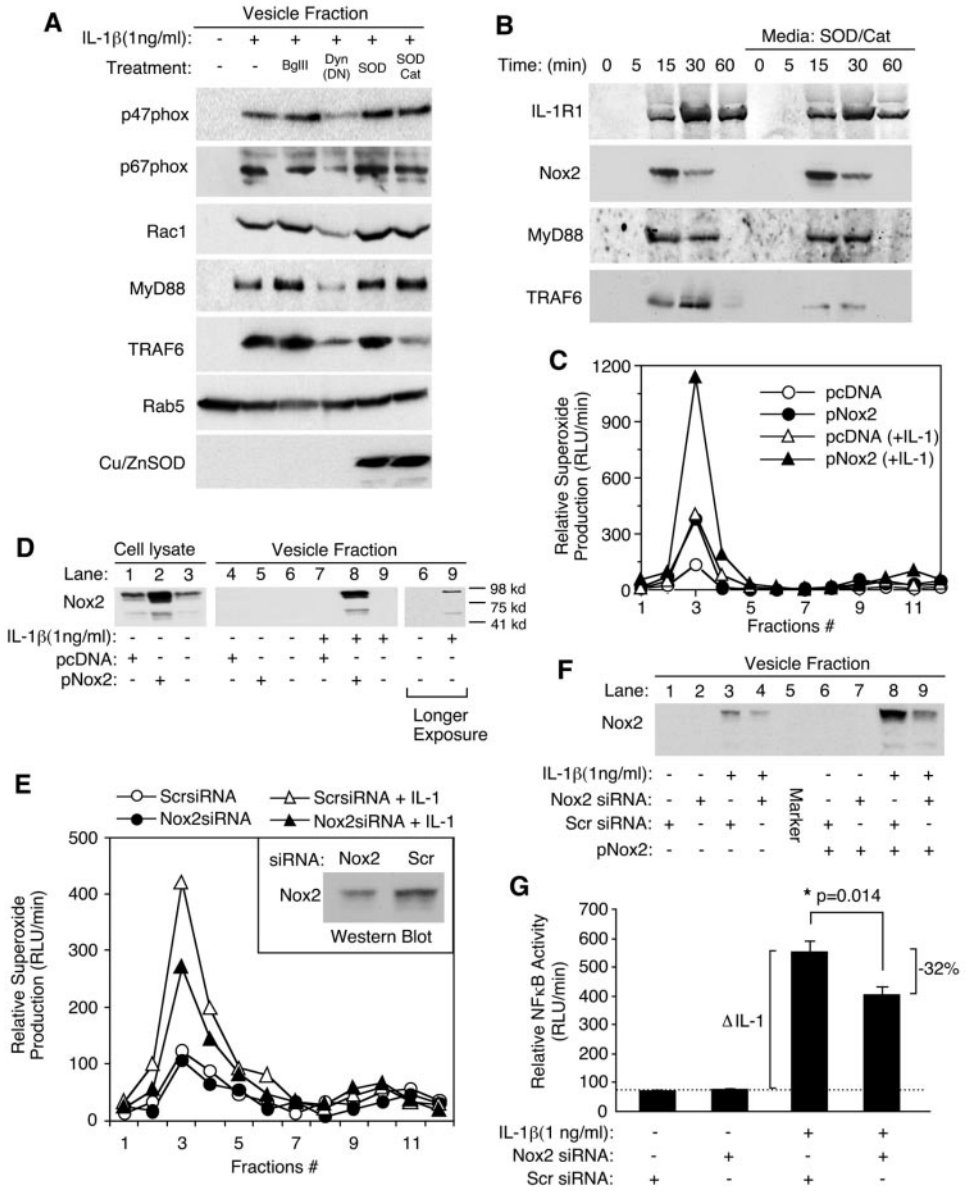

FIG. 3. Nox2 facilitates superoxide production in the endosomal compartment following IL-1β stimulation. (A) Western blot analysis of p47phox, p67phox, Rac1, MyD88, TRAF6, Rab5, and Cu/ZnSOD proteins in the isolated vesicular fraction of MCF-7 cells infected with Ad.BglII (control virus) or Ad.Dyn(DN) or treated with SOD and/or catalase proteins prior to IL-1β treatment for 20 min. (B) Time course of IL-1R1, Nox2, MyD88, and TRAF6 recruitment into the vesicular compartment following IL-1β treatment in the presence or absence of purified bovine Cu/ZnSOD and catalase proteins added to the medium. Isolated vesicular fractions were analyzed by Western blotting for the indicated proteins at various times post-IL-1β stimulation. (C and D) MCF-7 cells were transfected with a Nox2 expression plasmid (pNox2) or an irrelevant plasmid (pcDNA). At 48 h posttransfection, cells were stimulated with IL-1β and vesicular fractions were isolated at 20 min poststimulation. (C) NADPH-dependent $\cdot O_2^-$ production by Iodixanol gradient fractions following transfection with the indicated constructs. (D) Western blotting evaluating Nox2 expression in whole-cell lysates and isolated peak vesicular fractions 2 to 4 (longer exposures of lanes 6 and 9 detect endogenous levels of Nox2). Fully processed Nox2 migrates at ~95 kDa. (E and F) MCF-7 cells were transfected with Nox2 siRNA or a scrambled (Scr) control siRNA 48 h prior to IL-1β treatment. (E) NADPH-dependent $\cdot O_2^-$ production of Iodixanol gradient fractions following transfection with the indicated siRNA constructs. Inset depicts Western blot expression of total cellular endogenous Nox2 protein from cells transfected with Nox2 siRNA or scrambled siRNA. (F) Western blotting for Nox2, evaluating the effect of Nox2 or scrambled siRNA transfection on the recruitment of endogenous Nox2 (lanes 1 to 4), or transfected Nox2 (from a pNox2 expression plasmid) (lanes 6 to 9), into the peak Iodixanol vesicular fractions (2 to 4). (G) MCF-7 cells were transfected with Nox2 or scrambled siRNAs 48 h prior to IL-1β treatment. Transfected cells were then infected with Ad.NFκBLuc 24 h prior to IL-1β treatment. NF-κB transcriptional activity was then assessed at 5 h following IL-1β stimulation by quantifying luciferase activity in 5 μg of protein lysate (mean ± SE; $n = 6$). *, Student's t test demonstrated a significant reduction (32%) in IL-1β-stimulated NF-κB activity in the presence of Nox2 siRNA compared to scrambled siRNA. The dotted line demonstrates the baseline NF-κB activity prior to IL-1β stimulation.

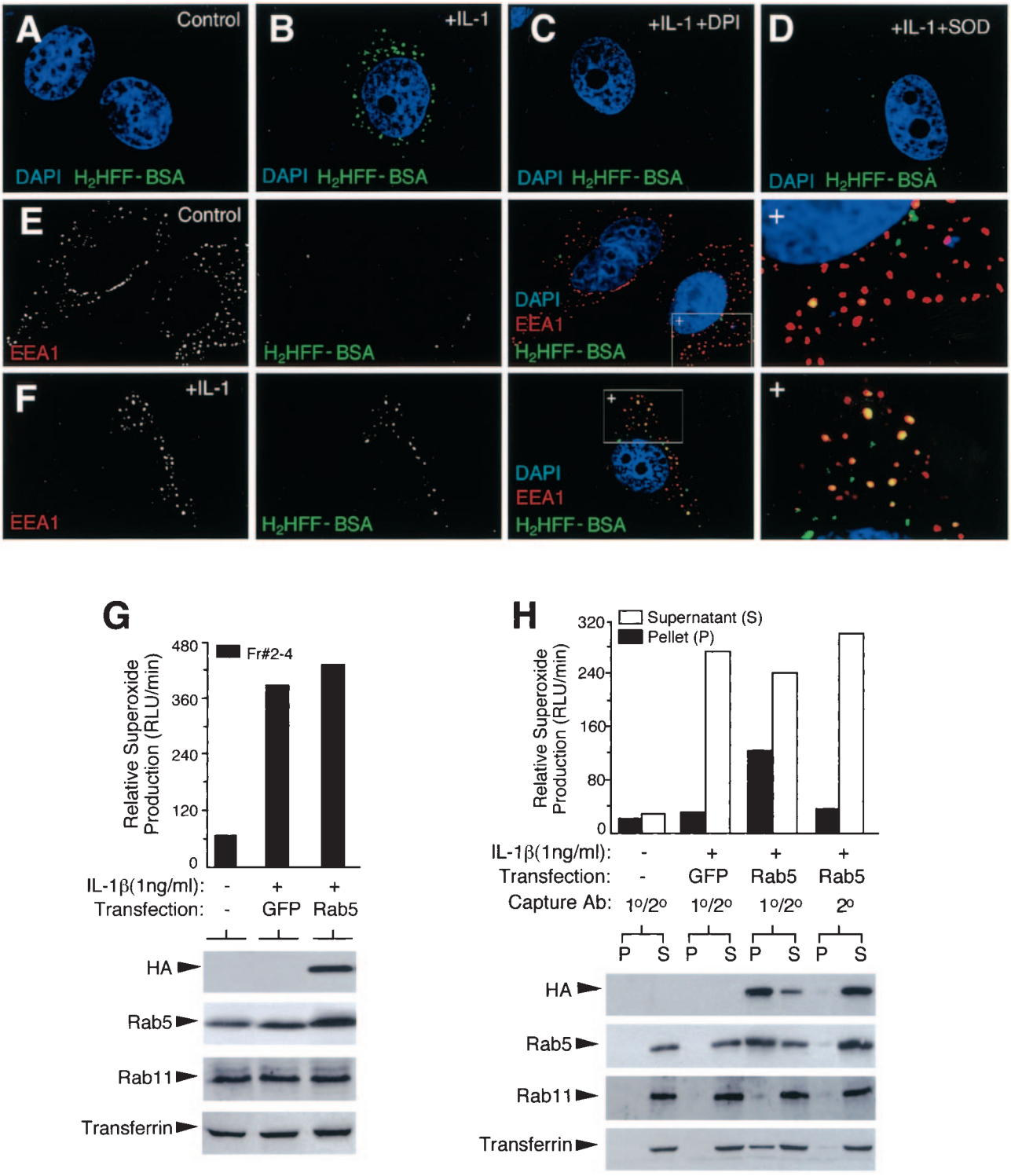

FIG. 4. IL-1β induces $\cdot O_2^-$ production by the early endosome compartment. (A to D) Endosomal $\cdot O_2^-$ production in MCF-7 cells was visualized by H_2HFF-BSA endosomal loading following a 10-min IL-1β (1.0 ng/ml) stimulation. Treatment conditions are indicated in the upper-right corner of each panel. H_2HFF-BSA, IL-1β, DPI, and/or SOD was added at the time of IL-1β stimulation. Control cells were treated with vehicle (PBS). DAPI was included in the mounting medium for localization of the nucleus. Green staining denotes $\cdot O_2^-$ production as fluorescent H_2HFF. (E and F) Localization of EEA1 in MCF-7 cells treated with PBS (E) or IL-1β (F) in the presence of H_2HFF-BSA for 10 min, followed by fixation. Anti-EEA1 was detected using a Texas Red secondary antibody, and slides were mounted in DAPI-containing medium. Black-and-white photomicrographs for each row depict the indicated EEA1 or H_2HFF-BSA fluorescent channels. Combined three-color images are given, with the right-most panel being an enlargement of the boxed region marked with a +. Three types of vesicles are seen: red, EEA1 positive; yellow, EEA1 positive $\cdot O_2^-$ producing; green, $\cdot O_2^-$ producing non-EEA1 reactive. (G) MCF-7 cells were transfected with HA-Rab5 or GFP expression plasmids 48 h prior to IL-1β and biotin-transferrin treatment for 20 min. Vesicular peak fractions (Fr #2 to 4) were evaluated for NADPH oxidase activity and Western blotting for HA, Rab5, Rab11, or avidin-horseradish peroxidase. (H) Immuno-affinity isolation of HA-Rab5-associated endosomes using half of the vesicular peak fractions (2 to 4) shown in panel G. Dynabeads used for immuno-affinity isolation were coated with primary anti-HA antibody and/or secondary antibody, as indicated. Both the pellets (P) and supernatants (S) were evaluated for NADPH oxidase activity and Western blotted following immuno-affinity isolation, as for panel G. Equal percentages of the original sample were evaluated in panels G and H.

HA-Rab5 compartment (Dynabead pellet) following IL-1β stimulation. This activity represented approximately one-third of the total NADPH oxidase activity in the starting fraction. The specificity of this isolation procedure was confirmed by several criteria. First, no significant contamination of Rab11 recycling endosomes was seen in the purified Rab5 endosomal fractions. Second, Dynabeads coated with the secondary antibody alone, or isolated with both primary and secondary antibodies from control GFP-transfected cells, demonstrated only low background levels of Nox activity associated with the beads. The integrity of Rab5-isolated endosomes was also confirmed by the retention of intravesicular biotin-transferrin loaded at the time of IL-1β treatment. Considering the efficiency of the HA affinity isolation (~75%) (Fig. 4H, anti-HA Western blot), these results suggested that at least half of the redox-active endosomes were Rab5-associated early endosomes at the time point evaluated (20 min). Given the fact that the Rab5 compartment is the earliest endosomal compartment to form following receptor endocytosis, these studies also support the hypothesis that Nox2 is recruited from the plasma membrane into the redox-active endosomes.

Rac1 and MyD88 both control the formation of redox-active endosomes, TRAF6 recruitment to IL-1R1, and NF-κB activation following IL-1β stimulation. Our data thus far have demonstrated that IL-1β stimulation leads to the formation of redox-active endosomes containing Nox2 complex subunits (Nox2, Rac1, p47phox, and p67phox). ROS generation by these Nox2-active endosomes was critical for the recruitment of TRAF6, but not MyD88, to vesicular membranes (Fig. 2H). Given that Nox2 activation in the endosomal compartment required active endocytosis (Fig. 2G), we reasoned that internalization of IL-1β-bound IL-1R1 coordinates the recruitment of the Nox2 catalytic subunit into the endosome. However, currently there are no reports describing the molecular determinants for IL-1R1 internalization following ligand binding. For example, although MyD88 is known to be one of the first effectors to recruit to IL-1R1 following ligand binding and is essential for NF-κB activation by IL-1R1 (1), it is unclear if MyD88 is essential for receptor internalization following ligand binding. Furthermore, previous studies have suggested that Rac1 associates with the IL-1R1 complex through an interaction with MyD88 (21). Since Rac1 is known to be part of the active Nox2 complex, we reasoned that Rac1 might recruit the Nox2 into IL-1R1-containing endosomes through its interaction with the receptor complex at the plasma membrane. Our findings, demonstrating that IL-1β stimulation promotes $\cdot O_2^-$ production in EEA1/Rab5-positive early endosomes (Fig. 4), also support the hypothesis that Nox2 (an integral membrane protein) enters the endosomal compartment very early from the plasma membrane.

To investigate the contribution of MyD88 and Rac1 in the internalization of IL-1R1 and the formation of redox-active endosomes, we developed RNA inhibition (RNAi) strategies to inhibit both MyD88 and Rac1 expression. As shown in Fig. 5A, transfection of siRNA targeting either MyD88 or Rac1 effectively inhibited their expression at the protein level. Such inhibition was not observed with a scrambled siRNA control. As predicted from previous studies in MyD88-deficient cells (1), NF-κB activation was significantly inhibited by MyD88 siRNA (Fig. 5B). Interestingly, Rac1 siRNA also inhibited NF-κB activation to a similar extent as seen with MyD88 siRNA. However, simultaneous transfection of both MyD88 and Rac1 siRNA did not provide additive inhibition of NF-κB, compared to either siRNA alone, suggesting that the two factors act on the same pathway to activate NF-κB by IL-1β. Furthermore, MyD88 or Rac1 siRNA inhibited $\cdot O_2^-$ production by the endosomal compartment following IL-1β challenge (Fig. 5C); however, Rac1 siRNA provided a slightly greater level of inhibition. These findings suggested that both MyD88 and Rac1 were critical for NF-κB activation and Nox2 activation in the endosomal compartment following IL-1β stimulation.

We next investigated whether Rac1 indeed associated with IL-1R1 and, if so, whether this interaction was dependent on MyD88. Indeed, we observed that Rac1 does associate with immunoprecipitated IL-1R1 following ligand simulation (Fig. 5D). However, in contrast to previous reports suggesting that Rac1 association with the IL-1R1 complex was dependent on MyD88 (21), we observed very little reduction in Rac1 association with IL-1R1 when MyD88 levels were significantly reduced by RNAi (Fig. 5D). Similarly, Rac1 siRNA reduced Rac1, but not MyD88, association with IL-1R1 (Fig. 5E). These findings suggest that MyD88 and Rac1 associate independently with IL-1R1 following ligand stimulation. However, RNAi inhibition of either MyD88 or Rac1 abrogated TRAF6 recruitment to the receptor complex (Fig. 5D and E). This finding is consistent with the fact that RNAi against MyD88 or Rac1 inhibited the formation of redox-active endosomes and NF-κB activation (Fig. 5B and C). Given the fact that endosomal ROS was important for TRAF6 recruitment to endosomes following IL-1β stimulation (Fig. 2H), these studies suggest that MyD88 and Rac1 are two critical factors involved in the formation of redox-active endosomes, an event required for the redox-dependent recruitment of TRAF6 to IL-1R1 and NF-κB activation.

To determine the roles that MyD88 and Rac1 play in the formation of redox-active endosomes, we sought to dissect the contributions of these two factors on internalization of the receptor and Nox2 into redox-active endosomes. We reasoned that MyD88 played a major role in initiating endocytosis of the receptor following ligand binding, while Rac1 was responsible for recruiting Nox2 into endosomes harboring the ligand-bound receptor. MCF-7 cells were transfected with MyD88 or Rac1 siRNA, and the recruitment of IL-1R1, MyD88, TRAF6, Rac1, and Nox2 into the endomembrane fraction was evaluated by Western blotting (Fig. 5F). Findings from these studies demonstrated that MyD88 inhibition by RNAi significantly attenuated internalization of IL-1R1 and the recruitment of MyD88, TRAF6, Rac1, and Nox2 to endomembranes (Fig. 5F). These findings suggest that the inhibition of MyD88 abrogates the formation of redox-active endosomes following IL-1β stimulation in a similar fashion to dynaminK44A (Fig. 2G), by preventing receptor-mediated endocytosis of Rac1/Nox2 complexes into the endosomal compartment. In contrast to MyD88 siRNA, Rac1 siRNA did not inhibit IL-1R1/MyD88 internalization following ligand stimulation, but rather significantly inhibited the recruitment of Rac1, Nox2, and TRAF6 to the endosomal compartment (Fig. 5F). These findings, together with the redox dependency of TRAF6 recruitment to the endosomal compartment (Fig. 2H), suggest that Rac1 plays

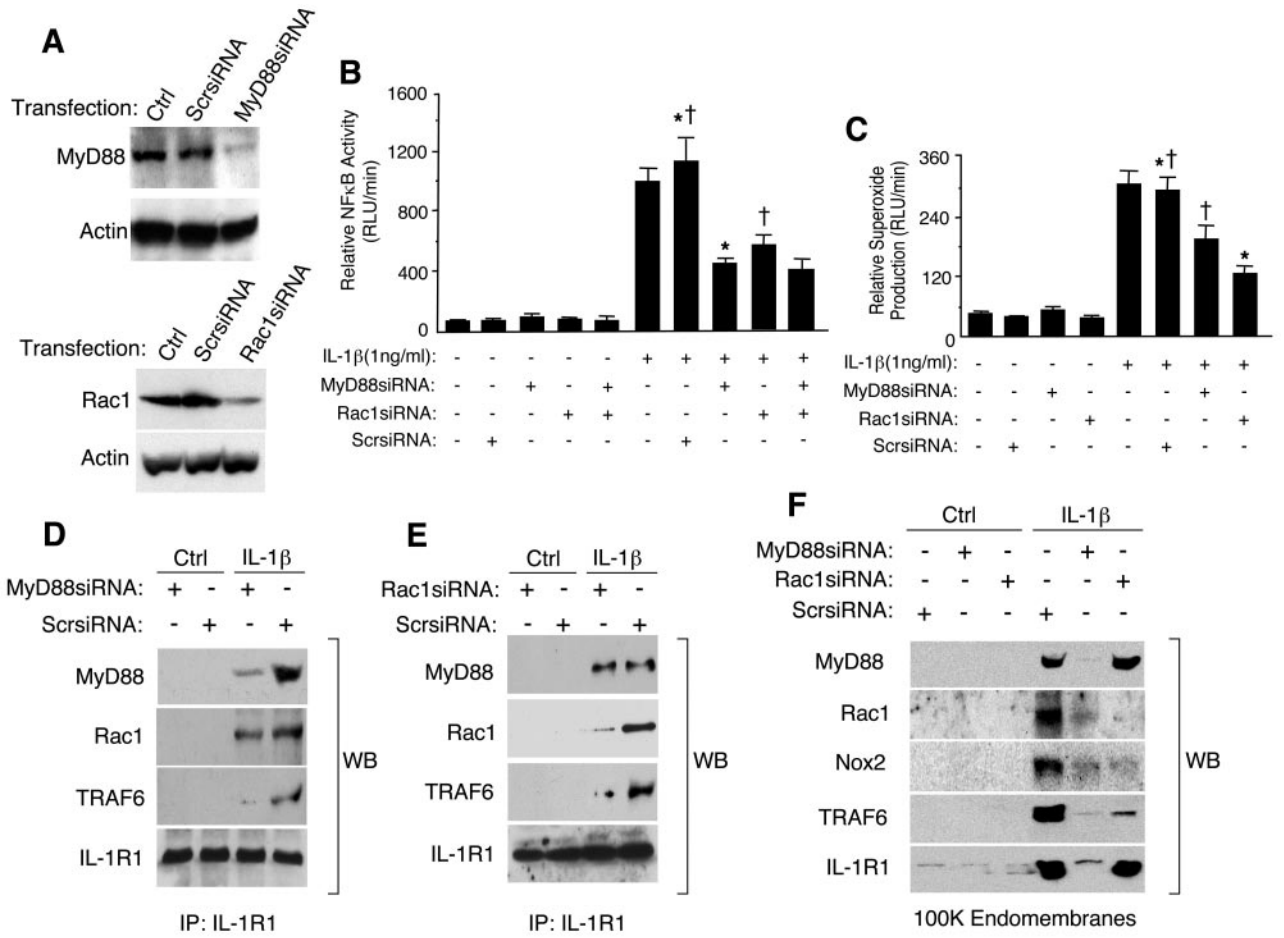

FIG. 5. Rac1 recruits Nox2 into the endosomal compartment by associating with IL-1R1 and is required for efficient redox-dependent recruitment of TRAF6 to the endosomal IL-1R1/MyD88 complex. (A) MCF-7 cells were transfected with MyD88 siRNA, Rac1 siRNA, or a scrambled (Scr) siRNA 48 h prior to examining MyD88 or Rac1 expression by Western blotting. (B) MCF-7 cells were transfected with the indicated siRNAs, infected with Ad.NFκBLuc prior to IL-1β stimulation, and analyzed for luciferase activities at 6 h post-cytokine treatment (mean ± standard error [SE]; $n = 3$). Paired comparisons (*, †) demonstrate significant differences ($P < 0.05$). (C) MCF-7 cells were transfected with the indicated siRNAs prior to a 20-min IL-1β stimulation and analysis of NADPH-dependent $\cdot O_2^-$ production in the peak Iodixanol vesicular fractions (mean ± SE; $n = 3$). Paired comparisons (*, †) demonstrate significant differences ($P < 0.05$). (D and E) MCF-7 cells were transfected with the indicated siRNAs prior to IL-1β stimulation for 20 min. IL-1R1 was then immunoprecipitated from cell lysates, followed by Western blotting for MyD88, Rac1, TRAF6, and IL-1R1. (F) MCF-7 cells were transfected with the indicated siRNAs and stimulated with IL-1β for 20 min, and PNS were generated. An enriched endomembrane fraction was generated by centrifugation of PNS at 100,000 × *g* for 2 h. The endomembrane pellets were collected and evaluated for MyD88, Rac1, Nox2, TRAF6, and IL-1R1 by Western blotting.

a critical role in recruiting TRAF6 to endosomal ligand-activated IL-1R1 by facilitating the recruitment/activation of Nox2 in the endosomal compartment. Cumulatively, these studies indicate that both MyD88 and Rac1 play critical roles in establishing the formation of redox-active endosomes by coordinating endocytosis of the receptor and recruitment of Nox2, respectively. Both processes are important for effective recruitment of TRAF6 to the ligand-activated IL-1R1 in the endosomal compartment and IKK/NF-κB activation following IL-1β stimulation.

MyD88 binds to IL-1R1 at the plasma membrane, while TRAF6 is recruited to endosomal IL-1R1 in an H_2O_2-dependent fashion. Our findings demonstrate for the first time that MyD88 is essential for IL-1R1 internalization into the endosomal compartment and suggest that MyD88 is recruited to the plasma membrane following ligand binding and prior to receptor internalization. Furthermore, recruitment of MyD88 to IL-1β-activated endosomes was not dependent on the endosomal redox state (Fig. 2H and 3A and B). In contrast, our studies demonstrate that TRAF6 recruitment to IL-1β-activated endosomes was dependent on ROS production by the endosomal compartment (Fig. 2H and 3A and B). These findings suggested that IL-1R1 recruitment of TRAF6 might occur in a redox-dependent fashion at the level of the endosome. Furthermore, since both catalase and SOD endosomal loading were required to efficiently block IL-1β-mediated TRAF6 endosomal recruitment and IKK activation (Fig. 3A and B and 1D), we hypothesized that Nox2-derived H_2O_2 was necessary for the recruitment of TRAF6 to the endosome. To investigate this hypothesis, we sought to evaluate the extent to which MyD88 and TRAF6 were recruited to IL-1R1 in the plasma membrane and endosomal compartments following ligand

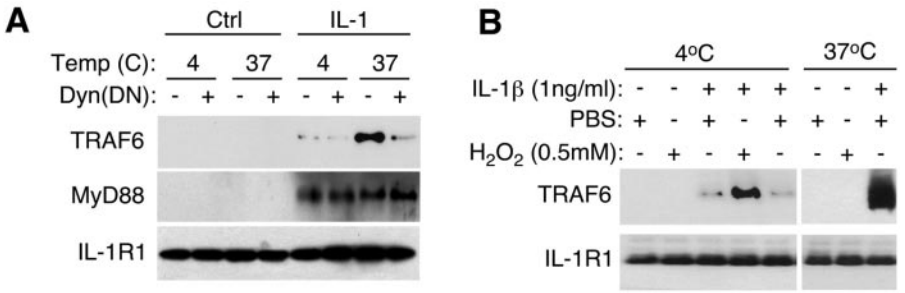

FIG. 6. TRAF6 recruitment to endosomal IL-1R1 is dependent on H_2O_2. (A) MCF-7 cells were infected with AdDyn(DN) or AdBglII (negative control). At 48 h postinfection, cells were treated with IL-1β at either 4°C (1 h) or 37°C (20 min). IL-1R1 was then immunoprecipitated, followed by Western blotting for the indicated proteins. (B) Cells were treated with IL-1β at 4°C (1 h) or 37°C (20 min) in the presence or absence of H_2O_2. IL-1R1 was then immunoprecipitated, followed by Western blotting for the indicated proteins.

binding and the extent to which these processes were dependent on H_2O_2.

To evaluate the recruitment of MyD88 and TRAF6 to IL-1R1 in the plasma membrane, we performed experiments under conditions in which endocytosis was blocked (at 4°C) or significantly inhibited by dynamin(K44A) expression. Results from these experiments confirmed that inhibiting endocytosis significantly impaired TRAF6, but not MyD88, recruitment to immunoprecipitated ligand-activated IL-1R1 (Fig. 6A). For example, in the absence of endocytosis at 4°C, TRAF6 was unable to bind to IL-1R1 following IL-1β stimulation, while MyD88 binding was similar to that seen at 37°C. Interestingly, the redox-dependent recruitment of TRAF6 to IL-1R1 could be reconstituted at the plasma membrane in the absence of endocytosis by the addition of exogenous H_2O_2; 500 μM H_2O_2 effectively promoted recruitment of TRAF6 to only ligand-activated IL-1R1 at the plasma membrane at 4°C (Fig. 6B). Such findings provide new insights into several aspects of IL-1R1 activation. First, they demonstrate that TRAF6 effector recruitment to ligand-activated IL-1R1 predominantly occurs at the level of the endosome. Second, they demonstrate that H_2O_2 is likely the ROS that facilitates TRAF6 recruitment to ligand-activated IL-1R1. Third, they provide a physiologic framework for Nox2 activation in endosomes as the source of H_2O_2 for this recruitment process.

Endosomal ROS enhance IL-1β-dependent activation of IKK by the endosomal compartment. Ligand activation of IL-1R1 facilitates IKK activation through the recruitment of at least two potential IKK kinases (TAK1 and/or NIK) to its receptor-associated effector complex (16). Once the IKK complex is phosphorylated by the activated receptor complex, IKK is activated to phosphorylate IκBα/β and NF-κB is mobilized to the nucleus. To better understand how redox-active endosomes functionally regulate NF-κB activation, we next investigated whether isolated IL-1β-stimulated endosomes could directly activate the IKK complex (Fig. 7A). This in vitro reconstitution assay utilized isolated vesicular fractions and immunoprecipitated IKK complex as kinase activation sources and phosphorylation of GST-IκBα as the molecular marker of IKK activation. We first sought to confirm that endosomes isolated from the IL-1β-treated cells could activate immunoprecipitated IKK complex from naive cells. As shown in Fig. 7B, this was indeed the case. Immunoprecipitated IKK complex from non-IL-1β-treated cells was activated to phosphorylate GST-IκBα in the presence of IL-1β-activated endosomes (lane 5). No activation was seen in the presence of unstimulated endosomes (lane 4). Moreover, loading of both SOD and catalase into IL-1β-activated endosomes significantly inhibited their ability to activate IKK (lane 9), while SOD loading alone had little effect (lane 8). These findings provide direct evidence for the importance of endosomal-derived ROS in the activation of IKK and are consistent with H_2O_2 being the primary ROS required for TRAF6 recruitment to the receptor complex (Fig. 6B). Similarly, expression of dynamin(K44A) also inhibited vesicular IKK activation (lane 7), as would be expected since dynamin(K44A) inhibited the formation of redox-active endosomes and recruitment of TRAF6 to IL-1R1 (Fig. 2G, 3A, and 6A). Interestingly, a low level of GST-IκBα phosphorylation was observed with IL-1β-activated endosomes in the absence of immunoprecipitated naive IKK complex (lane 6). This finding suggests that the IKK complex may only transiently associate with the activated receptor complex on redox-active endosomes. Such a finding is similar to IκBα/IKK complex interactions, which demonstrate that IκBα dissociates from the IKK complex once it is phosphorylated on S32/S36 (39).

DISCUSSION

Endocytosis has long been regarded as a classical mechanism for down-regulating receptor-mediated signaling at the plasma membrane. However, increasing evidence has indicated that endocytosis also plays an important role in the activation, amplification, and sorting of membrane-initiated receptor signals (44). Here we describe a new redox-dependent mechanism of receptor activation linked to Nox2 activation and ROS production by the early endosomal compartment. The identification of Nox2-active endosomes following IL-1β stimulation provided a framework for understanding how ROS can influence IL-1 receptor activation of NF-κB. Although the concept of ROS involvement in the activation of NF-κB remains controversial (19), several reports have implicated H_2O_2 as a key mediator in IL-1β and TNF-α activation of NF-κB by demonstrating inhibition with overexpressed glutathione peroxidase (25, 29). Findings from our present study have elucidated the series of events that control IL-1R1 endocytosis following ligand binding and the subsequent H_2O_2-dependent recruitment of TRAF6 to the MyD88/IL-1R1 complex in the endosomal compartment. This redox-dependent process was

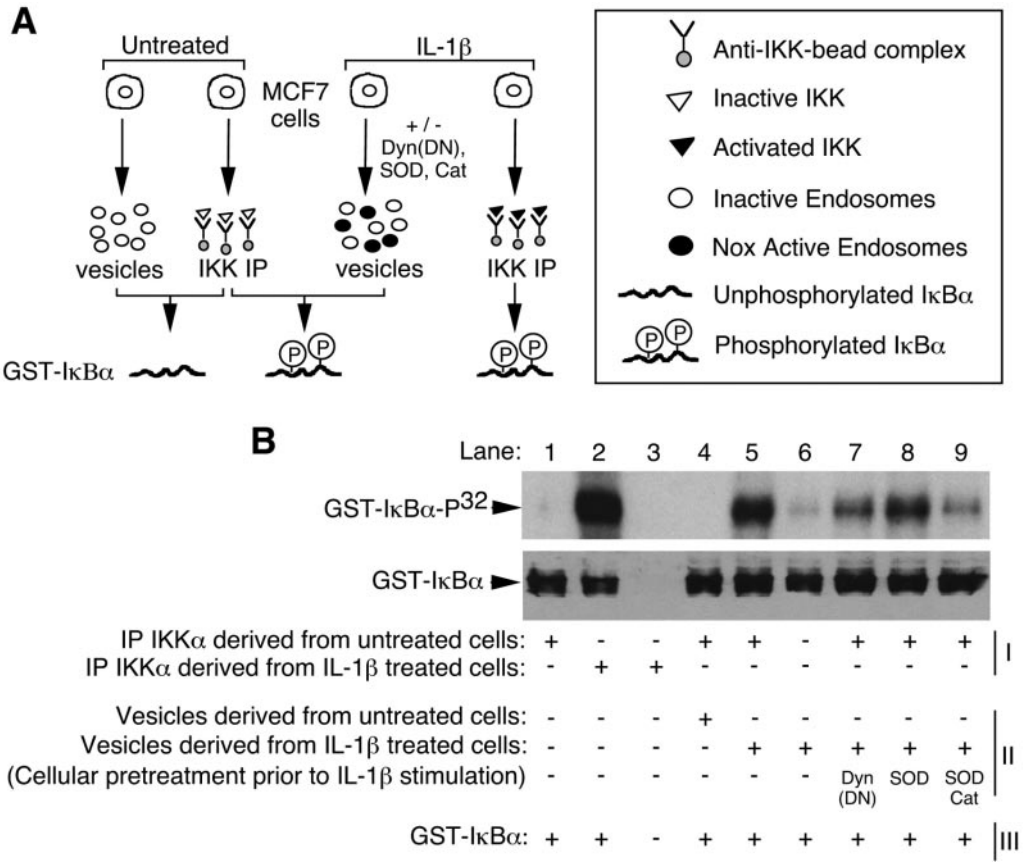

FIG. 7. IL-1β-stimulated redox-active endosomes activate the IKK complex. (A) Strategy for evaluating IKK activation by redox-active endosomes in an in vitro reconstitution assay. (B) IKK assays for kinase activity were performed using in vitro reconstitution of three components: (i) immunoprecipitated IKKα, (ii) isolated vesicles, and/or (iii) GST-IκBα as a substrate. Vesicles and immunoprecipitated (IP) IKK were isolated from untreated or IL-1β-treated MCF-7 cells. Three additional treatments were performed prior to IL-1β stimulation and isolation of vesicles. These included infection with Ad.Dyn(DN) or treatment with SOD and/or catalase proteins. Components I to III were combined, as indicated, in the presence of [γ-^{32}P]ATP. GST-IκBα phosphorylation was evaluated by SDS-PAGE autoradiography (top panel). Western blotting using an anti-GST antibody was then performed to confirm equal loading of GST-IκBα (bottom panel).

necessary for efficient activation of the IKK complex and NF-κB.

Our studies have focused on determining the molecular events that control Nox2 activation in the endosomal compartment following IL-1β stimulation (Fig. 8). In this regard, endocytosis of ligand-activated IL-1R1 was necessary for efficient Nox2 complex activation and production of ROS by the endosomal compartment. This process was a major controlling event responsible for the redox-dependent recruitment of TRAF6 to ligand-activated endosomal IL-1R1 effector complexes and subsequent IKK activation. Rac1 binding to IL-1R1 appeared to play a central role in mediating Nox2 recruitment into the endosomal compartment following IL-1β stimulation. Rac1 has predominantly been thought to play an essential role in Nox2 activation by recruiting p67phox to the Nox complex (11). Our studies demonstrate for the first time that Rac1 can also serve to localize Nox2 to the proper cellular compartment with a ligand-activated receptor. In contrast to MyD88, Rac1 did not appear to be required for endocytosis of IL-1R1 following ligand binding. However, both effectors contributed to Nox activation in the endosomal compartment and, hence, the redox-dependent recruitment of TRAF6 to IL-1R1. In summary, inhibition of MyD88 reduced Nox2 activation and TRAF6 recruitment in the endosomal compartment by inhibiting endocytosis of ligand-activated IL-1R1 (in a similar fashion to dynaminK44A). In contrast, Rac1 inhibition likely reduced Nox2 activation in the endosomal compartment by preventing Nox2 tethering to ligand-activated IL-1R1. However, it is presently unclear if Rac1 binds directly to the receptor or through a secondary unknown effector (other than MyD88).

Oxidation of thiol groups is recognized as a mechanism to induce redox-dependent changes in protein function (15, 22). Given the ability of H_2O_2 to directly promote TRAF6 recruitment to ligand-activated IL-1R1 at the plasma membrane (at 4°C) and essentially bypass the need for endocytic formation of redox-active endosomes, we currently hypothesize that oxidation of thiol groups in TRAF6, or an upstream effector such as IRAK, leads to a redox-dependent change in protein structure that allows for effector recruitment to the IL-1R1/MyD88 complex. Other scenarios are also possible, such as redox-dependent changes in MyD88 and/or IL-1R1 that facilitate efficient docking of IRAK/TRAF6 complexes. Alternatively, IRAK/TRAF6 association with IL-1R1 could also be controlled indi-

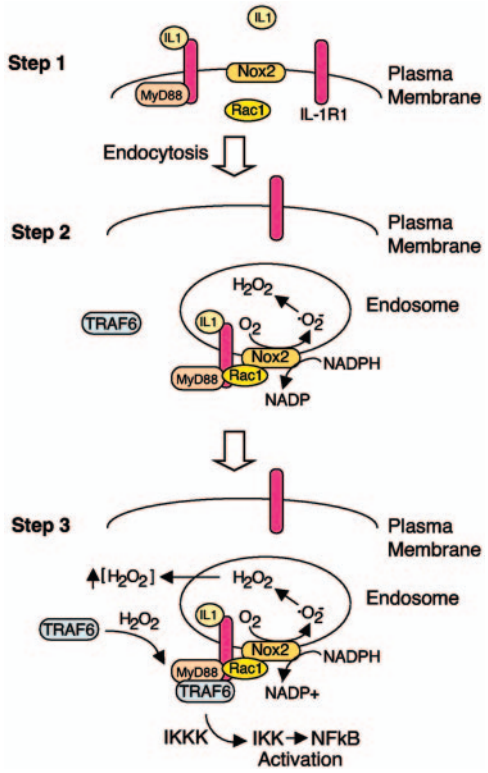

FIG. 8. Summary of IL-1R1 receptor complex activation and its dependence on endosomal ROS. Schematically drawn is a model of three major steps in IL-1R1 complex formation following binding of IL-1β. (Step 1) Binding of IL-1β to IL-1R1 on the plasma membrane triggers MyD88 and Rac1 association with the receptor. Rac1 was required for the recruitment of Nox2 into the endosomal compartment, while MyD88 was required to initiate endocytosis of the receptor. Since IL-1β stimulation promotes $\cdot O_2^-$ production in EEA1/Rab5-positive early endosomes (Fig. 4), our data support the hypothesis that Nox2 (an integral membrane protein) enters the endosomal compartment very early (i.e., from the plasma membrane). However, other scenarios are also possible, such as fusion of Nox2-containing vesicles with early endosomes containing ligand-activated IL-1R1. (Step 2) MyD88 association with IL-1R1 triggers endocytosis of MyD88/Rac1/Nox2, with IL-1R1 leading to NADPH-dependent $\cdot O_2^-$ production by the endosomal compartment. Spontaneous dismutation of $\cdot O_2^-$ to H_2O_2 likely gives rise to increased H_2O_2 both inside and outside the endosome, since H_2O_2 is permeable to membranes (2). (Step 3) Local increases in H_2O_2 facilitate the redox-dependent association of TRAF6 with the receptor complex on ligand-activated endosomes. The binding of TRAF6 to the receptor complex leads to activation of downstream IKK kinases (IKKK), IKK and, ultimately, NF-κB.

rectly through ROS regulation of kinases or phosphatases with a catalytic cysteine(s). In support of this latter hypothesis, IRAK phosphorylation by protein kinase C has been shown to be critical for IRAK autophosphorylation and NF-κB activation by IL-1β (33).

Nox proteins are known to be a major source of ROS within cells following various environmental stimuli (26); however, their function in regulating cellular signaling has only recently been recognized. For example, Nox4 appears to be important in ROS-mediated insulin signaling (32), and Nox1 mediates angiotensin II redox-sensitive signaling pathways (18, 27). Here we describe for the first time that Nox2 can regulate IL-1β signaling and describe the mechanism responsible for this redox-dependent regulation in the context of NF-κB activation. Our findings also provide new insights into the subcellular context in which Nox activation occurs and selectively influences H_2O_2-dependent receptor activation in the endosomal compartment. It is plausible that the presently studied mechanism defining the influences of endosomal Nox-derived ROS on IL-1R1 activation may also have overlapping characteristics with other redox-dependent receptor signaling pathways. For example, PDGF signaling is controlled by H_2O_2 and receptor-associated peroxiredoxin II, which acts to eliminate H_2O_2 as the site of receptors and influence PDGF receptor phosphatases (7). ROS production following PDGF stimulation is also controlled by Rac1 and has been suggested to involve NADPH oxidases (4). Hence, although our studies in mammary epithelial cells have implicated endosomal Nox2 in IL-1β signaling, it is possible that other cell types also utilize this mechanism for other redox-regulated signal transduction pathways in conjunction with Rac1-dependent Nox isoforms.

ACKNOWLEDGMENTS

This work was supported by NIDDK (DK067928 and DK51315) (J.F.E.) as well as a grant from The Center for Gene Therapy (P30 DK54759). J.F.E. holds the Roy J. Carver Chair of Molecular Medicine.

We also gratefully acknowledge Michael Welsh for helpful discussions, Leah Williams for editorial assistance, and Sean Martin and Garry Buettner from the ESR facility. We also thank J. D. Lambeth for a Nox2 expression plasmid and A. Jesaitis for a Nox2 antibody.

REFERENCES

1. **Akira, S., and K. Hoshino.** 2003. Myeloid differentiation factor 88-dependent and -independent pathways in toll-like receptor signaling. J. Infect. Dis. **187**(Suppl. 2)**:**S356–S363.
2. **Antunes, F., and E. Cadenas.** 2000. Estimation of H_2O_2 gradients across biomembranes. FEBS Lett. **475:**121–126.
3. **Bae, Y. S., S. W. Kang, M. S. Seo, I. C. Baines, E. Tekle, P. B. Chock, and S. G. Rhee.** 1997. Epidermal growth factor (EGF)-induced generation of hydrogen peroxide. Role in EGF receptor-mediated tyrosine phosphorylation. J. Biol. Chem. **272:**217–221.
4. **Bae, Y. S., J. Y. Sung, O. S. Kim, Y. J. Kim, K. C. Hur, A. Kazlauskas, and S. G. Rhee.** 2000. Platelet-derived growth factor-induced H_2O_2 production requires the activation of phosphatidylinositol 3-kinase. J. Biol. Chem. **275:** 10527–10531.
5. **Burns, K., J. Clatworthy, L. Martin, F. Martinon, C. Plumpton, B. Maschera, A. Lewis, K. Ray, J. Tschopp, and F. Volpe.** 2000. Tollip, a new component of the IL-1RI pathway, links IRAK to the IL-1 receptor. Nat. Cell Biol. **2:**346–351.
6. **Burritt, J. B., M. T. Quinn, M. A. Jutila, C. W. Bond, and A. J. Jesaitis.** 1995. Topological mapping of neutrophil cytochrome b epitopes with phage-display libraries. J. Biol. Chem. **270:**16974–16980.
7. **Choi, M. H., I. K. Lee, G. W. Kim, B. U. Kim, Y. H. Han, D. Y. Yu, H. S. Park, K. Y. Kim, J. S. Lee, C. Choi, Y. S. Bae, B. I. Lee, S. G. Rhee, and S. W. Kang.** 2005. Regulation of PDGF signalling and vascular remodelling by peroxiredoxin II. Nature **435:**347–353.
8. **Coligan, J. E.** 1991. Current protocols in immunology. Greene Publishing Associates and Wiley-Interscience, New York, N.Y.
9. **Conner, S. D., and S. L. Schmid.** 2003. Regulated portals of entry into the cell. Nature **422:**37–44.
10. **Deshpande, S. S., P. Angkeow, J. Huang, M. Ozaki, and K. Irani.** 2000. Rac1 inhibits TNF-alpha-induced endothelial cell apoptosis: dual regulation by reactive oxygen species. FASEB J. **14:**1705–1714.
11. **Diekmann, D., A. Abo, C. Johnston, A. W. Segal, and A. Hall.** 1994. Interaction of Rac with p67phox and regulation of phagocytic NADPH oxidase activity. Science **265:**531–533.
12. **Duan, D., Q. Li, A. W. Kao, Y. Yue, J. E. Pessin, and J. F. Engelhardt.** 1999. Dynamin is required for recombinant adeno-associated virus type 2 infection. J. Virol. **73:**10371–10376.
13. **Engelhardt, J. F.** 1999. Redox-mediated gene therapies for environmental injury: approaches and concepts. Antioxid. Redox. Signal. **1:**5–27.
14. **Frey, R. S., A. Rahman, J. C. Kefer, R. D. Minshall, and A. B. Malik.** 2002. PKCζ regulates TNF-α-induced activation of NADPH oxidase in endothelial cells. Circ. Res. **90:**1012–1019.

15. **Georgiou, G.** 2002. How to flip the (redox) switch. Cell **111:**607–610.
16. **Ghosh, S., and M. Karin.** 2002. Missing pieces in the NF-κB puzzle. Cell **109**(Suppl)**:**S81–S96.
17. **Gu, Y., Y. C. Xu, R. F. Wu, F. E. Nwariaku, R. F. Souza, S. C. Flores, and L. S. Terada.** 2003. p47phox participates in activation of RelA in endothelial cells. J. Biol. Chem. **278:**17210–17217.
18. **Hanna, I. R., Y. Taniyama, K. Szocs, P. Rocic, and K. K. Griendling.** 2002. NAD(P)H oxidase-derived reactive oxygen species as mediators of angiotensin II signaling. Antioxid. Redox. Signal. **4:**899–914.
19. **Hayakawa, M., H. Miyashita, I. Sakamoto, M. Kitagawa, H. Tanaka, H. Yasuda, M. Karin, and K. Kikugawa.** 2003. Evidence that reactive oxygen species do not mediate NF-κB activation. EMBO J. **22:**3356–3366.
20. **Huang, J., X. Gao, S. Li, and Z. Cao.** 1997. Recruitment of IRAK to the interleukin 1 receptor complex requires interleukin 1 receptor accessory protein. Proc. Natl. Acad. Sci. USA **94:**12829–12832.
21. **Jefferies, C., A. Bowie, G. Brady, E. L. Cooke, X. Li, and L. A. O'Neill.** 2001. Transactivation by the p65 subunit of NF-κB in response to interleukin-1 (IL-1) involves MyD88, IL-1 receptor-associated kinase 1, TRAF-6, and Rac1. Mol. Cell. Biol **21:**4544–4552.
22. **Kamata, H., S. I. Honda, S. Maeda, L. Chang, H. Hirata, and M. Karin.** 2005. Reactive oxygen species promote TNF-α-induced death and sustained JNK activation by inhibiting MAP kinase phosphatases. Cell **120:**649–661.
23. **Kanai, F., H. Liu, S. J. Field, H. Akbary, T. Matsuo, G. E. Brown, L. C. Cantley, and M. B. Yaffe.** 2001. The PX domains of p47phox and p40phox bind to lipid products of PI_3K. Nat. Cell Biol. **3:**675–678.
24. **Kang, S. W., T. S. Chang, T. H. Lee, E. S. Kim, D. Y. Yu, and S. G. Rhee.** 2004. Cytosolic peroxiredoxin attenuates the activation of Jnk and p38 but potentiates that of Erk in Hela cells stimulated with tumor necrosis factor-alpha. J. Biol. Chem. **279:**2535–2543.
25. **Kretz-Remy, C., P. Mehlen, M. E. Mirault, and A. P. Arrigo.** 1996. Inhibition of I kappa B-alpha phosphorylation and degradation and subsequent NF-kappa B activation by glutathione peroxidase overexpression. J. Cell Biol. **133:**1083–1093.
26. **Lambeth, J. D.** 2004. NOX enzymes and the biology of reactive oxygen. Nat. Rev. Immunol. **4:**181–189.
27. **Lassegue, B., D. Sorescu, K. Szocs, Q. Yin, M. Akers, Y. Zhang, S. L. Grant, J. D. Lambeth, and K. K. Griendling.** 2001. Novel $gp91^{phox}$ homologues in vascular smooth muscle cells: nox1 mediates angiotensin II-induced superoxide formation and redox-sensitive signaling pathways. Circ. Res. **88:**888–894.
28. **Li, J. M., A. M. Mullen, S. Yun, F. Wientjes, G. Y. Brouns, A. J. Thrasher, and A. M. Shah.** 2002. Essential role of the NADPH oxidase subunit $p47^{phox}$ in endothelial cell superoxide production in response to phorbol ester and tumor necrosis factor-alpha. Circ. Res. **90:**143–150.
29. **Li, Q., S. Sanlioglu, S. Li, T. Ritchie, L. Oberley, and J. F. Engelhardt.** 2001. GPx-1 gene delivery modulates NFκB activation following diverse environmental injuries through a specific subunit of the IKK complex. Antioxid. Redox. Signal. **3:**415–432.
30. **Li, S., A. Strelow, E. J. Fontana, and H. Wesche.** 2002. IRAK-4: a novel member of the IRAK family with the properties of an IRAK-kinase. Proc. Natl. Acad. Sci. USA **99:**5567–5572.
31. **Li, Y., H. Zhu, P. Kuppusamy, V. Roubaud, J. L. Zweier, and M. A. Trush.** 1998. Validation of lucigenin (bis-*N*-methylacridinium) as a chemilumigenic probe for detecting superoxide anion radical production by enzymatic and cellular systems. J. Biol. Chem. **273:**2015–2023.
32. **Mahadev, K., H. Motoshima, X. Wu, J. M. Ruddy, R. S. Arnold, G. Cheng, J. D. Lambeth, and B. J. Goldstein.** 2004. The NAD(P)H oxidase homolog Nox4 modulates insulin-stimulated generation of H_2O_2 and plays an integral role in insulin signal transduction. Mol. Cell. Biol. **24:**1844–1854.
33. **Mamidipudi, V., C. Lin, M. L. Seibenhener, and M. W. Wooten.** 2004. Regulation of interleukin receptor-associated kinase (IRAK) phosphorylation and signaling by iota protein kinase C. J. Biol. Chem. **279:**4161–4165.
34. **Muzio, M., J. Ni, P. Feng, and V. M. Dixit.** 1997. IRAK (Pelle) family member IRAK-2 and MyD88 as proximal mediators of IL-1 signaling. Science **278:**1612–1615.
35. **O'Neill, L. A., and C. Greene.** 1998. Signal transduction pathways activated by the IL-1 receptor family: ancient signaling machinery in mammals, insects, and plants. J. Leukoc. Biol. **63:**650–657.
36. **Pagano, P. J., J. K. Clark, M. E. Cifuentes-Pagano, S. M. Clark, G. M. Callis, and M. T. Quinn.** 1997. Localization of a constitutively active, phagocyte-like NADPH oxidase in rabbit aortic adventitia: enhancement by angiotensin II. Proc. Natl. Acad. Sci. USA **94:**14483–14488.
37. **Park, H. S., S. H. Lee, D. Park, J. S. Lee, S. H. Ryu, W. J. Lee, S. G. Rhee, and Y. S. Bae.** 2004. Sequential activation of phosphatidylinositol 3-kinase, beta Pix, Rac1, and Nox1 in growth factor-induced production of H_2O_2. Mol. Cell. Biol. **24:**4384–4394.
38. **Qian, Y., M. Commane, J. Ninomiya-Tsuji, K. Matsumoto, and X. Li.** 2001. IRAK-mediated translocation of TRAF6 and TAB2 in the interleukin-1-induced activation of NF-κB. J. Biol. Chem. **276:**41661–41667.
39. **Regnier, C. H., H. Y. Song, X. Gao, D. V. Goeddel, Z. Cao, and M. Rothe.** 1997. Identification and characterization of an IκB kinase. Cell **90:**373–383.
40. **Rhee, S. G., Y. S. Bae, S. R. Lee, and J. Kwon.** 2000. Hydrogen peroxide: a key messenger that modulates protein phosphorylation through cysteine oxidation. Sci. STKE **53:**1–6.
41. **Rhee, S. G., T. S. Chang, Y. S. Bae, S. R. Lee, and S. W. Kang.** 2003. Cellular regulation by hydrogen peroxide. J. Am. Soc. Nephrol. **14:**S211–S215.
42. **Rothwarf, D. M., and M. Karin.** 1999. The NF-kappa B activation pathway: a paradigm in information transfer from membrane to nucleus. Sci. STKE **1999:**RE1.
43. **Sanlioglu, S., C. M. Williams, L. Samavati, N. S. Butler, G. Wang, P. B. McCray, Jr., T. C. Ritchie, G. W. Hunninghake, E. Zandi, and J. F. Engelhardt.** 2001. Lipopolysaccharide induces Rac1-dependent reactive oxygen species formation and coordinates tumor necrosis factor-alpha secretion through IKK regulation of NF-kappa B. J. Biol. Chem. **276:**30188–30198.
44. **Sorkin, A., and M. Von Zastrow.** 2002. Signal transduction and endocytosis: close encounters of many kinds. Nat. Rev. Mol. Cell Biol. **3:**600–614.
45. **Sundaresan, M., Z. X. Yu, V. J. Ferrans, K. Irani, and T. Finkel.** 1995. Requirement for generation of H_2O_2 for platelet-derived growth factor signal transduction. Science **270:**296–299.
46. **Trischler, M., W. Stoorvogel, and O. Ullrich.** 1999. Biochemical analysis of distinct Rab5- and Rab11-positive endosomes along the transferrin pathway. J. Cell Sci. **112:**4773–4783.
47. **Van Buul, J. D., M. Fernandez-Borja, E. C. Anthony, and P. L. Hordijk.** 2005. Expression and localization of NOX2 and NOX4 in primary human endothelial cells. Antioxid. Redox. Signal. **7:**308–317.
48. **Wang, C., L. Deng, M. Hong, G. R. Akkaraju, J. Inoue, and Z. J. Chen.** 2001. TAK1 is a ubiquitin-dependent kinase of MKK and IKK. Nature **412:**346–351.
49. **Wesche, H., W. J. Henzel, W. Shillinglaw, S. Li, and Z. Cao.** 1997. MyD88: an adapter that recruits IRAK to the IL-1 receptor complex. Immunity **7:**837–847.
50. **Xiao, L., D. R. Pimentel, J. Wang, K. Singh, W. S. Colucci, and D. B. Sawyer.** 2002. Role of reactive oxygen species and NAD(P)H oxidase in alpha(1)-adrenoceptor signaling in adult rat cardiac myocytes. Am. J. Physiol. Cell Physiol. **282:**C926–C934.
51. **Zerial, M., and H. McBride.** 2001. Rab proteins as membrane organizers. Nat. Rev. Mol. Cell Biol. **2:**107–117.